frontiers in Earth Science

ORIGINAL RESEARCH
published: 19 August 2021
doi: 10.3389/feart.2021.736054

Influence of a Paleosedimentary Environment on Shale Oil Enrichment: A Case Study on the Shahejie Formation of Raoyang Sag, Bohai Bay Basin, China

Yongbo Wei[1,2], Xiaoyan Li[3], Ruifeng Zhang[3], Xiaodong Li[3], Shuangfang Lu[1,2], Yan Qiu[3], Tao Jiang[3], Yuan Gao[3], Tiedong Zhao[3], Zhaojing Song[1,2] and Meihong Zhao[4]*

[1]Shandong Provincial Key Laboratory of Deep Oil and Gas, Qingdao, China, [2]School of Geosciences, China University of Petroleum (East China), Qingdao, China, [3]Research Institute of Exploration and Development, PetroChina Huabei Oilfield Company, Renqiu, China, [4]Downhole Operation Branch of Bohai Drilling Engineering Co. LTD, PetroChina, Renqiu, China

OPEN ACCESS

Edited by:
Guochang Wang,
Saint Francis University, United States

Reviewed by:
Yinhui Zuo,
Chengdu University of Technology, China
Zaixing Jiang,
China University of Geosciences, China

***Correspondence:**
Shuangfang Lu
lushuangfang@upc.edu.cn

Specialty section:
This article was submitted to Economic Geology, a section of the journal Frontiers in Earth Science

Received: *04 July 2021*
Accepted: *09 August 2021*
Published: *19 August 2021*

Citation:
Wei Y, Li X, Zhang R, Li X, Lu S, Qiu Y, Jiang T, Gao Y, Zhao T, Song Z and Zhao M (2021) Influence of a Paleosedimentary Environment on Shale Oil Enrichment: A Case Study on the Shahejie Formation of Raoyang Sag, Bohai Bay Basin, China. Front. Earth Sci. 9:736054. doi: 10.3389/feart.2021.736054

The characteristics of paleosedimentary environments are of great significance for the enrichment of organic matter (OM) and hydrocarbons in lacustrine shale. This study analyzed mineralogy, well logging data, organic geochemical parameters (total organic carbon and pyrolyzed hydrocarbon), inorganic geochemical parameters (major and trace elements), and multiple geochemical proxies based on inorganic geochemical parameters. These were used to reconstruct the paleosedimentary environment of the lower 1st Member of the Shahejie Formation (Es_1^L) to reveal OM and shale oil enrichment mechanisms and establish a shale oil enrichment model. The $(Fe_2O_3+Al_2O_3)/(CaO + MgO)$, Sr/Ba, Rb/Sr, Cu/Al, and Th/U parameters indicate that the Es_1^L in Raoyang Sag was deposited in a paleoenvironment dominated by arid paleoclimate, reducing conditions, and saltwater. Paleoclimate, clastic influx intensity, preservation conditions, paleoproductivity, and paleosalinity all affect OM abundance. The OM accumulation in the shale of Es_1^L was mainly controlled by the high primary productivity of surface water due to algal blooms and moderate salinities, which was achieved using stratified water columns with low oxygen conditions in bottom water. As the main valuable sites for shale oil storage, carbonate mineral depositions are of great significance for oil enrichment. As the dominant lithofacies for oil enrichment, carbonate-rich shale and calcareous shale lithofacies were deposited under a drier paleoclimate, low clastic influx intensity, strong reducing conditions, high paleoproductivity, and moderate salinity paleoenvironment. Additionally, the profile of the shale oil sweet spot was determined through the combination of lithofacies, logging, and paleosedimentary environment data.

Keywords: paleoenvironment, OM accumulation, shale oil enrichment, Shahejie formation, Raoyang sag

INTRODUCTION

Lacustrine organic-rich mudstones and shale possess conditions conducive to hydrocarbon generation, requisite storage volumes, and excellent hydrocarbon-bearing properties. These types of oil and gas reservoirs have the characteristics of continuous and stable distribution in space, high overall oil and gas content, sweet spot enrichment, and high yield (Jarvie, 2012; Zhou et al., 2020; Wei et al., 2021; Wei et al., 2021). The theory of lacustrine shale oil accumulation is a hot research topic and is directly related to the properties of source rocks (Holditch, 2013; Zou et al., 2019; Feng et al., 2020; Li et al., 2021). According to sedimentology theory, the paleosedimentary environment has a particularly significant impact on continental sedimentation at different scales (mesoscale and macroscale) (Carroll and Bohacs, 1999). At the microscale of the lacustrine sedimentary sequence, there are broad differences in mineralogy, sedimentary structure, and lithofacies (Lu et al., 2016; Li et al., 2017; Bai et al., 2020). The vertical and horizontal distribution characteristics of the different types of shale deposited in basins also have significant variations stemming from differences in paleosedimentary environments. However, total organic carbon (TOC), shale oil-bearing layers, and reservoir quality are generally considered to be the main indicators for evaluating shale oil accumulation (Bai et al., 2020). The TOC of shale denotes its oil production potential (Holditch, 2013), whereas the existence of shale oil-bearing layers (Katz, 2003) is a good indicator of shale oil sweet spots. These parameters are closely related to the mineral composition, structures, and lithofacies formed in each type of sedimentary environment and have varying degrees of influence on shale oil enrichment; a fact that has recently drawn notice (Birdwell et al., 2016; Lu et al., 2016; Zou, 2017). Thus, revealing the relationship between the paleosedimentary environment and shale oil enrichment is highly significant to in-depth investigations into the enrichment mechanism of continental shale oil, which promotes the effective exploration and efficient extraction of shale oil resources. The establishment of the shale oil accumulation model also has relevant significance to similar lacustrine basins worldwide.

The Raoyang Sag in eastern China is a representative example of an oil-bearing lacustrine basin in the Jizhong Depression. The continental organic-rich shale in the lower 1st Member of the Shahejie Formation (Es_1^L) is one of the most important source rocks in the Raoyang Sag and even in the entire Bohai Bay Basin. Recently, it has been considered as a potential shale oil reservoir (Yin et al., 2018; Chen et al., 2019a; Chen et al., 2019b; Yin et al., 2020). Previous research has focused on the characteristics of organic geochemical properties [e.g., TOC, pyrolyzed hydrocarbon (S_1)] (Chen et al., 2019a; Chen et al., 2019b; Yin et al., 2020), physical properties of shale oil reservoirs (pore characterization and storage space classification) (Chen et al., 2019a; Chen et al., 2019b), and the paleoenvironment developed through the organic and inorganic geochemistry of the Es_1^L source rocks (Yin et al., 2018; Yin et al., 2020). However, research on the inorganic and organic geochemical enrichment mechanisms of organic matter (OM) under the shale oil enrichment model of the Es_1^L in Raoyang Sag is relatively weak.

The paleosedimentary environment and shale oil enrichment model can be constructed by combining mineralogy and inorganic geochemistry. Based on the organic and inorganic geochemical parameters of four key wells in the study area, this study conducted a systematic study of the shale oil enrichment mechanism and mainly focused on the following four aspects: 1) determination of the mineralogy, organic geochemistry, and major/trace element characteristics of the Es_1^L shale; 2) reconstruction of the paleoenvironment (including clastic influx, paleoclimate, paleosalinity, redox conditions, and paleoproductivity) during the deposition of Es_1^L shale; 3) analysis of the factors influencing OM abundance and elucidating the mechanism of OM enrichment in the Es_1^L shale; and 4) confirmation of the sedimentary environment of dominant oil-bearing lithofacies and establishment of a shale oil enrichment model.

GEOLOGICAL SETTING

The Raoyang Sag is a Cenozoic fault-sag basin in the middle of the Jizhong Depression in the Bohai Bay Basin. This sag exploration area covers approximately $5.28 \times 10^3\ km^2$, enclosed by the Xianxian Uplift to the east, the Gaoyang Low Uplift to the west, the Hengshui Fault to the south, and the Baxian Sag to the north. It is further subdivided into four oil-rich sags from north to south, namely, the Renxi, Maxi, Hejian, and Liuxi Sags, which house the largest oil and gas accumulations and the highest exploration effectiveness in the Raoyang Sag (He et al., 2017a; Yin et al., 2020) (**Figure 1A**). The strata of the Raoyang Sag are mainly composed of Paleozoic, Mesozoic, and Cenozoic rocks, from bottom to top. The Paleogene in Cenozoic rocks is generally thick and includes the Kongdian, Shahejie, and Dongying formations (He et al., 2017b; Liang et al., 2018). Amidst these, the Es_1^L in Raoyang Sag has a large area of continuous distribution of organic-rich mudstones and shale that developed in semi-deep lake facies, mainly consisting of carbonate, clay, and silica minerals (e.g., quartz and feldspar). The lithology of the middle and upper parts of the interval are complex, composed of dark gray mudstone, calcareous shale, oil shale, dolomitic mudstone, fine sandstone, and oolitic limestone. It is called "special lithology sections (SLC)". The lower part comprises "tailing sandstone (TS)," composed of fine siltstone (**Figure 1B**). This part has the appropriate geological conditions for shale oil to form an integrated source and reservoir and has good prospects for shale oil exploration.

SAMPLES AND METHODS

Samples

Core observations and 96 shale samples were collected from depths between 2,332.00 and 3,827.92 m from 14 wells in the Raoyang Sag (**Figure 1A**). Four of these wells (wells B11x, Xl25x, N202, and G103), especially wells B11x and Xl25x, have been continuously cored, and the collected samples provide a large volume of important data for analyzing the paleoenvironmental OM enrichment and shale oil accumulation in the Es_1^L.

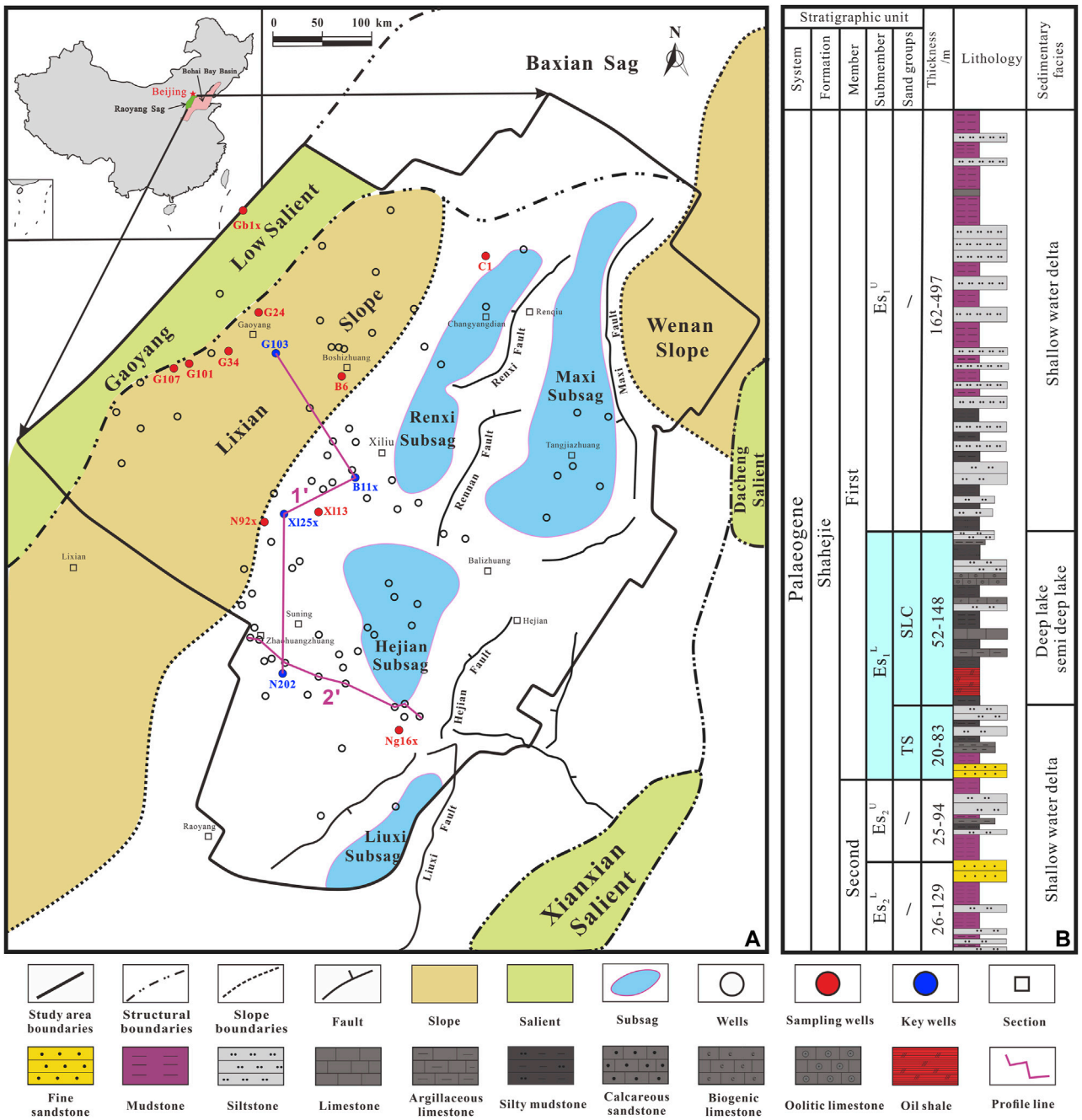

FIGURE 1 | (A) Map showing the structural characteristics within and around the Raoyang Sag and the distribution of sampling wells **(B)** Stratigraphic column of the Shahejie Formation.

Moreover, these four wells are located in different structural positions and deposition depths of the lacustrine basins and exhibit a continuous organic-rich shale interval that can reflect the continuous paleoenvironmental evolution of the Es_1^L shale.

TOC and Rock-Eval Pyrolysis Analyses

TOC and Rock-Eval pyrolysis analyses were conducted at the Key Laboratory of Deep Oil and Gas at the China University of Petroleum (East China). A total of 96 samples of from 14 wells were analyzed to obtain TOC content. Samples were crushed to an approximate mesh size of 100 and oven-dried at 80°C. The TOC content was determined using an Elab-TOC/E2000 analyzer after decarbonating with hydrochloric acid (5%). Ninety-six crushed samples (approximately 100 mg at a mesh size of 80) from the 14 wells were analyzed using a YQ-VIIA Rock-Eval instrument, by heating at a programmed rate. Then, a flame

ionization detector and thermal conductivity detector were used to quantify the hydrocarbons and carbon dioxide emitted by the OM being released from the rock. The measured parameters included the free hydrocarbon content when vaporized at a temperature of 300°C (S_1), residual hydrocarbon generation potential when the temperature was between 300 and 600°C (S_2), and temperature of the maximum pyrolysis yield (T_{max}).

X-Ray Diffraction (XRD) Measurements

XRD analysis was performed on the 96 samples to quantitatively analyze mineral composition. All the shale samples were ground into a fine powder (<40 μm) and analyzed with a Panalytical X' PertPRO MPD X-ray with Cu Kα radiation (40 kV, 40 mA) at a scanning speed of 2°/min and a testing angle range of 5°–90°. The diffraction patterns were analyzed using a computer to determine the relative abundances of various minerals, and a semi-quantitative assessment was performed.

Major and Trace Element Determination

The major element compositions of 35 samples obtained from wells B11x, Xl25x, N202, and G103 were analyzed using a Philips PW2404 X-ray fluorescence spectrometer with fused glasses consisting of a mixture of powdered samples at a temperature of 1,000°C and flux ($Li_2B_4O_7$) at a ratio of 1:8 with a weight of 5.0 g. This analysis revealed major element oxides, including SiO_2, Al_2O_3, MgO, Na_2O, K_2O, P_2O_5, TiO_2, CaO, Fe_2O_3, and MnO. The precision of the major element data was ≤5%. The 35 sample powders (40 mg) that were selected for trace element analysis were dried in an oven at 130°C for 1–2 h, cooled to room temperature (20°C), dissolved in a tightly sealed Teflon screw-cap beaker with ultrapure 0.5 ml HNO_3 + 1 ml HF + 0.5 ml $HCLO_4$ with a solubility of 8 mol/L, and dried. The dried samples were digested again with 1 ml 1% HNO_3 +3 ml H_2O until a clear solution was obtained. The solution was then diluted to 1:1,000 by mass and analyzed using a Finnigan MAT inductively coupled plasma source mass spectrometer (ICP-MS) to measure trace and rare-earth elements. The testing error of these elements was generally less than 4%.

RESULTS

Organic Geochemical Characteristics

TOC content (obtained using the TOC analyzer) is one of the most important indicators for evaluating organic-rich shale. The TOC content of the shale samples from Es_1^L varied from 0.09 to 5.07% (mean 1.55%). In addition, S_1 is a direct parameter for determining the enrichment of shale oil. The mean S_1 value of the 96 samples from the Es_1^L was 0.65 mg HC/g rock (mg/g) (range: 0.01–6.27 mg/g). The (S_1 + S_2) values represent the OM hydrocarbon-generating potential. High (S_1 + S_2) values of up to 52.63 mg/g (average: 12.71 mg/g) indicate that the oil shales also have excellent potential for liquid hydrocarbon generation. According to the relationship between the hydrogen index (HI) and T_{max} (**Figure 2**), most of the measured oil shale samples belonged to Type I and Type II_1 kerogens, with a scant contribution of Type II_2 and III kerogens; This indicated that the OM of the shale samples had mainly algal and microorganism origins (Yin et al., 2020). The T_{max} parameter from the Rock-Eval pyrolysis data was investigated to evaluate the thermal maturity level of the OM. The T_{max} value (307–449°C; average: 434°C) indicated that the OM maturity stage ranged from immature to early mature (Shekarifard et al., 2019). This is due to the shale stratum in the Es_1^L not having experienced long-term burial and higher temperatures, due to the shallow burial depth of strata, a conclusion supported by the high (S_1+S_2) value.

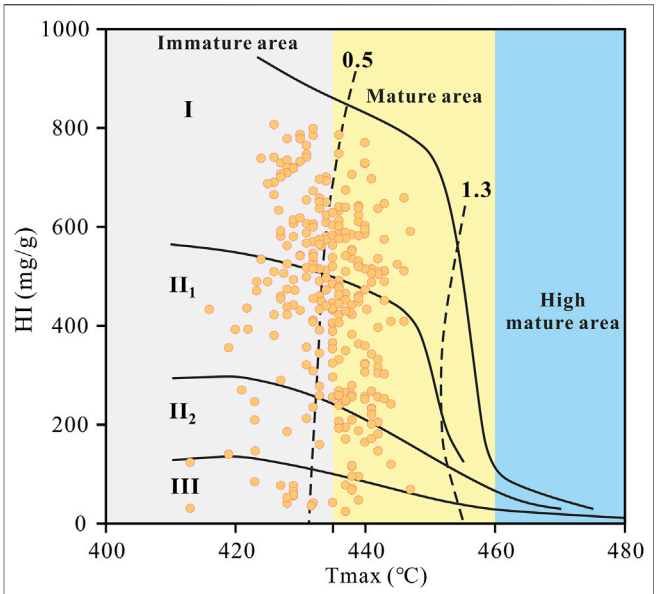

FIGURE 2 | Thermal maturity status and kerogen types (I, II_1, II_2, III) of the investigated Es1L shale samples, expressed by the relationship between HI and T_{max}.

Mineralogy and Lithofacies of Shale

XRD analysis of the 35 shale samples from the four selected wells indicated that the Es_1^L shale was dominated by carbonate (mean 35.21%), clay (mean 32.38%), and felsic (mean 32.42%) minerals (**Table 1**). Mineralogic information indicates that these rocks are not typical of shale (defined by clay mineral contents greater than 75%) (Schieber, 1989). The American Eagle Ford shale formation is generally rich in carbonates and hydrocarbons, and the Barnett shale formation is generally considered to be rich in quartz and oil (Slatt and Rodriguez, 2012; Chermak and Schreiber, 2014; He et al., 2017a). This mineralogical information also demonstrates that the carbonate minerals associated with these shales are of particular significance. In comparison, the mineral composition of the Es_1^L shale is closer to that of the Eagle Ford shale than the American black shale. Therefore, in references to the three-terminal (carbonate, clay, quartz, and feldspar) normalized lithofacies (Zhang et al., 2016; Zhou et al., 2020), shale with a carbonate content greater than 50% was defined as carbonate-rich shale. The color of the rock samples is dark-brown, with oil display, and obvious laminar structure of carbonate minerals and clay minerals. The existence of laminar structure indicates that there may be water stratification in ancient lakes (Larsen and Macdonald, 1993) (Area A in **Figures 3A**, **4A,B**), because the water stratification can

cause serious hypoxia in the bottom water, making it difficult for benthic animals to survive, so as to avoid the damage to the texture. Shale with a clay mineral content greater than 50% was defined as clay-rich shale. The rock sample is dark-brown with massive structure, and a small amount of terrigenous clastic minerals can be seen dispersed in clay minerals (Area B in **Figures 3A**, **4C,D**). Shale with a quartz and feldspar content greater than 50% was named felsic-rich shale. The rock sample is gray-yellow, compact and massive structure, and mainly composed of mixed sediments of clay minerals and fine-grained quartz or feldspar particles (Area C in **Figures 3A**, **4E,F**). Shale with three terminal elements less than 50% was defined as fine-grained hybrid shale. To further subdivide the lithofacies, the fine-grained hybrid shale was divided into calcareous shale (calcareous mineral content between 33.3 and 50%) (Area D in **Figures 3A**, **4G,H**), clay shale (clay minerals between 33.3 and 50%) (Area E in **Figures 3A**, **4I,J**), and felsic shale (felsic minerals between 33.3 and 50%) (Area F in **Figures 3A**, **4K,L**). Among them, the calcareous shale and clay shale are gray-brown, with oil display and laminar structure (interbedding of OM, clay minerals and carbonate minerals). The felsic shale is yellow-brown, compact and massive structure, and mainly composed of mixed sediments of clay minerals and fine silty quartz or feldspar particles. The lithofacies of the Es_1^L in Raoyang Sag mainly comprise carbonate-rich shale, clay-rich shale, felsic-rich shale, calcareous shale, clay shale, and felsic shale (**Figure 3A**). In addition, B11x well and Xl25x well mainly develop carbonate-rich shale, calcareous shale, and clay shale. N202 well and G103 well mainly develop felsic-rich shale and clay shale (**Table 1**). What needs to be distinguished is that this article discusses shale oil reservoirs, which are located in shale formations with thin interlayers of various lithologies such as dolomite and siltstone. In order to facilitate the unified study of shale oil reservoirs, we had classified the fine-grained sedimentary rocks in the shale formations as shale in the work of dividing lithofacies.

The clay mineral composition of shale samples from the four key wells is plotted in a three-terminal diagram (mixed-

TABLE 1 | XRD results and the corresponding geochemical parameters of the Es_1^L shale in the Roayang Sag.

Samples	Depth (m)	Minerals content (%)			TOC (%)	S_1 (mg/g)	S_1/TOC*100 (mg/g)	S_1+S_2 (mg/g)	T_{max} (°C)	Lithofacies
		Clay	Quartz and feldspar	Carbonate						
B11x-1	3,397.85	19.88	13.91	66.22	2.91	0.57	19.61	25.93	441	A
B11x-2	3,398.15	30.57	19.87	49.55	3.94	0.59	14.98	36.32	435	D
B11x-3	3,398.95	46.88	24.46	28.65	1.60	0.37	23.13	11.70	427	E
B11x-4	3,410.41	27.95	18.42	53.63	2.87	0.79	27.57	28.10	437	A
B11x-5	3,411.30	27.02	15.53	57.45	2.62	0.57	21.77	29.29	438	A
B11x-6	3,411.65	43.98	14.28	41.74	4.76	0.35	7.35	42.19	442	E
B11x-7	3,412.33	47.08	27.30	25.62	3.77	0.68	18.05	32.95	436	E
B11x-8	3,413.02	19.42	19.84	60.74	5.02	2.01	40.07	52.44	440	A
B11x-9	3,413.93	31.21	15.97	52.82	2.55	1.47	57.56	19.83	431	A
B11x-10	3,414.56	54.51	33.92	11.57	2.11	0.65	30.86	24.85	436	B
B11x-11	3,415.01	39.77	20.12	40.11	2.87	0.39	13.59	22.25	435	D
B11x-12	3,416.17	49.30	30.78	19.92	2.66	0.84	31.63	22.05	436	E
B11x-13	3,417.15	28.68	18.64	52.68	1.79	3.05	45.20	14.54	440	A
Xl25x-2	3,324.89	33.53	19.30	47.18	1.83	0.53	29.01	22.00	439	D
Xl25x-3	3,330.06	32.57	18.88	48.55	1.96	0.51	26.06	14.13	435	D
Xl25x-4	3,331.07	39.80	16.17	44.03	1.60	0.44	27.53	10.84	434	D
Xl25x-5	3,331.99	31.81	15.77	52.42	2.44	0.72	29.45	22.49	433	A
Xl25x-6	3,339.24	21.74	8.31	69.95	1.92	0.67	34.91	14.38	434	A
Xl25x-7	3,340.17	8.97	8.45	82.58	1.30	1.57	120.91	9.82	434	A
Xl25x-8	3,340.67	31.01	13.51	55.48	1.32	0.44	33.41	10.51	443	A
Xl25x-9	3,341.27	56.32	26.51	17.18	2.12	0.78	36.82	19.54	437	B
N202-7	3,560.68	37.00	29.54	33.46	3.55	0.41	11.57	33.19	446	E
N202-8	3,562.31	44.04	32.66	23.30	2.30	0.90	39.05	18.58	439	E
N202-9	3,563.56	37.38	18.20	44.42	2.13	0.88	41.25	17.64	441	D
N202-11	3,565.25	29.91	56.53	13.56	0.32	0.04	12.54	0.67	435	C
N202-13	3,569.90	17.75	72.05	10.20	0.32	0.03	9.34	0.57	436	C
N202-14	3,572.43	21.99	55.83	22.19	0.32	0.04	12.52	0.66	432	C
N202-15	3,575.35	7.77	72.12	20.11	0.38	0.93	242.87	3.78	429	C
G103-1	2,743.60	34.27	57.05	8.68	0.63	0.10	15.79	1.86	436	C
G103-2	2,744.80	24.08	59.54	16.38	0.18	0.02	11.08	0.24	432	C
G103-4	2,748.30	49.93	42.28	7.79	0.09	0.03	32.88	0.15	429	E
G103-5	2,749.80	11.97	71.57	16.46	0.25	0.03	11.99	1.02	437	C
G103-6	2,751.80	33.56	48.88	17.57	0.60	0.04	6.69	1.31	433	F
G103-7	2,754.10	50.88	34.29	14.84	0.45	0.04	8.80	1.20	437	B
G103-8	2,765.30	10.73	84.08	5.19	2.03	6.27	308.62	24.55	431	C

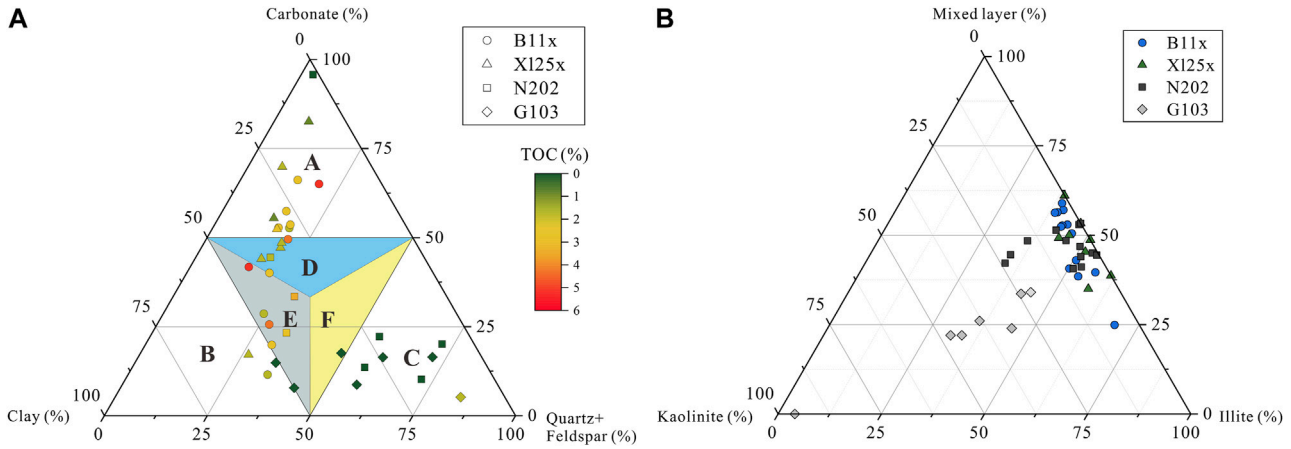

FIGURE 3 | Ternary plots of mineral composition from XRD data. **(A)**Ternary diagram of main mineral components [Carbonate-rich shale **(A)**, Clay-rich shale **(B)**, Felsic-rich shale **(C)**, Calcareous shale **(D)**, Clay shale **(E)**, Felsic shale **(F)**]. **(B)** Ternary diagram of clay mineral components.

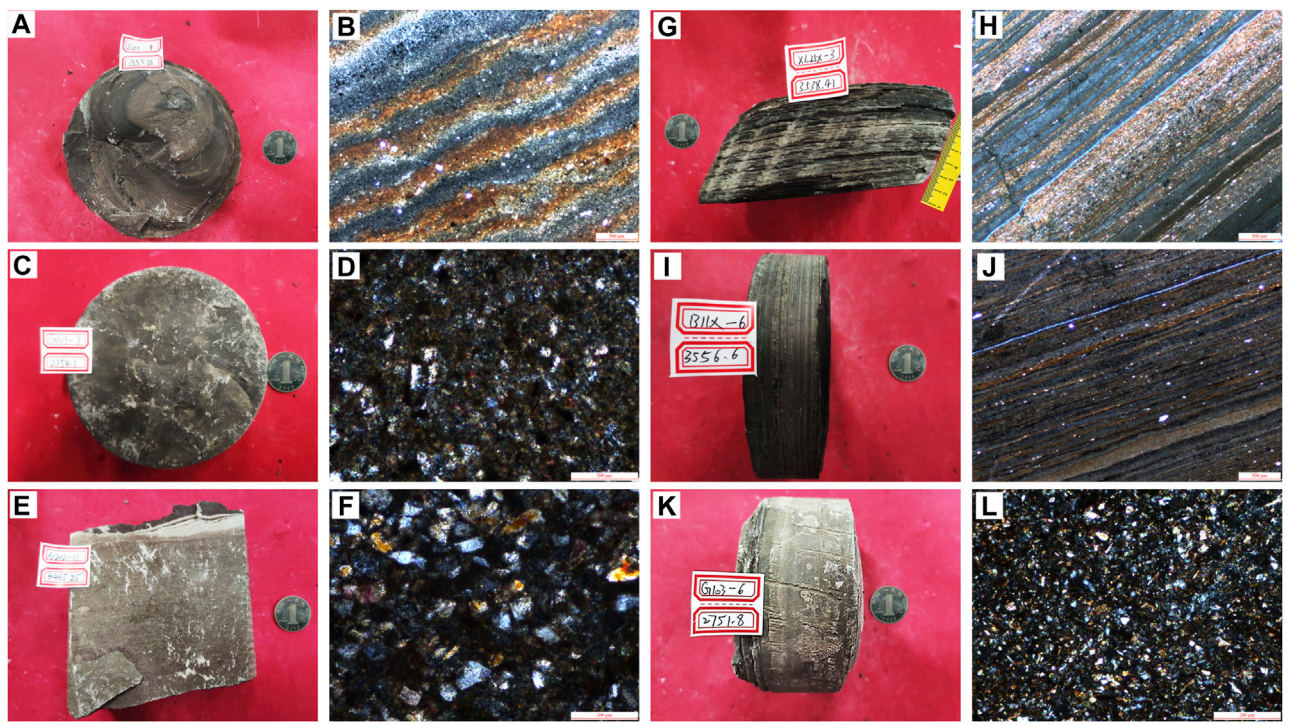

FIGURE 4 | (A,B): Carbonate-rich shale, B11x-4, 3,410.41 m; **(C,D)**: Clay-rich shale, G103-7, 2,754.10 m; **(E,F)**: Felsic-rich shale, N202-11, 3,565.25 m; **(G,H)**: Calcareous shale, Xl25x-3, 3,330.06 m; **(I,J)**: Clay shale, B11x-6, 3,411.65 m; **(K,L)**: Felsic shale, G103-6, 2,751.80 m.

layer illite/smectite, kaolinite, and illite) in **Figure 3B**. The clay minerals of the Es_1^L shale samples were composed of illite (avg. 43.46%), and mixed-layer illite/smectite (avg. 41.64%), with relatively small amounts of kaolinite (avg. 8.71%) and chlorite (avg. 6.19%). The clay minerals of the Es_1^L shale are rich in mixed-layer illite/smectite and illite, while the majority of the American shales are dominated by illite with little or no kaolinite (Loucks and Ruppel, 2007; Wilson et al., 2016). This may indicate that the evolution of the paleo-basin and paleosedimentary environment and the degree of diagenesis is different from that of American shale (Cai et al., 2015).

Geochemistry of Elements

The major element oxides SiO_2, CaO, and Al_2O_3 are the predominant constituents, with averages of 45.57 wt%,

TABLE 2 | Major elements results of the Es_1^L shale in the Raoyang Sag.

Samples	Depth (m)	SiO_2 (%)	Al_2O_3 (%)	MgO (%)	Na_2O (%)	K_2O (%)	P_2O_5 (%)	TiO_2 (%)	CaO (%)	Fe_2O_3 (%)	MnO (%)
B11x-1	3,397.85	29.24	7.59	3.56	1.19	1.58	0.16	0.35	24.72	3.00	0.06
B11x-2	3,398.15	37.71	9.08	3.43	1.20	1.86	0.13	0.40	19.31	3.48	0.08
B11x-3	3,398.95	48.72	12.12	3.21	1.44	2.66	0.20	0.57	10.46	4.71	0.07
B11x-4	3,410.41	42.20	9.59	2.64	1.27	1.86	0.10	0.39	18.94	4.26	0.10
B11x-5	3,411.30	44.62	11.86	4.26	1.43	2.48	0.11	0.52	11.58	4.75	0.06
B11x-6	3,411.65	37.82	9.87	4.49	1.34	2.06	0.16	0.43	16.08	4.83	0.08
B11x-7	3,412.33	46.72	11.87	2.39	1.43	2.49	0.13	0.56	12.57	4.34	0.06
B11x-8	3,413.02	37.96	8.35	1.74	1.10	1.51	0.23	0.34	24.67	3.92	0.10
B11x-9	3,413.93	38.14	9.17	1.77	1.31	1.78	0.09	0.37	21.61	2.82	0.03
B11x-10	3,414.56	42.93	9.83	3.73	1.43	2.03	0.11	0.41	16.26	3.30	0.07
B11x-11	3,415.01	42.23	10.71	2.08	1.23	2.38	0.10	0.44	17.84	3.55	0.07
B11x-12	3,416.17	50.58	12.37	2.61	1.41	2.76	0.09	0.52	10.40	5.41	0.08
B11x-13	3,417.15	36.22	8.66	1.62	1.26	1.80	0.10	0.36	23.39	2.83	0.06
Xl25x-2	3,324.89	43.06	10.61	2.97	1.37	2.23	0.10	0.47	15.55	4.57	0.06
Xl25x-3	3,330.06	40.72	10.65	1.95	1.48	2.20	0.09	0.47	19.46	2.20	0.03
Xl25x-4	3,331.07	37.68	9.68	1.84	1.50	1.93	0.08	0.42	22.36	2.76	0.05
Xl25x-5	3,331.99	40.06	9.59	2.03	1.26	1.94	0.15	0.39	20.96	4.05	0.08
Xl25x-6	3,339.24	28.24	7.48	2.51	0.91	1.89	0.23	0.31	29.41	2.39	0.10
Xl25x-7	3,340.17	17.08	4.40	4.22	0.56	0.82	0.26	0.15	33.09	2.41	0.13
Xl25x-8	3,340.67	30.45	7.92	3.73	1.02	1.94	0.12	0.33	23.57	3.71	0.12
Xl25x-9	3,341.27	38.12	9.83	4.37	1.26	2.46	0.13	0.48	18.35	3.53	0.10
N202-7	3,560.68	47.03	12.87	2.66	1.43	2.82	0.11	0.56	12.05	5.11	0.10
N202-8	3,562.31	46.22	11.92	2.65	1.11	3.13	0.09	0.51	14.39	3.24	0.05
N202-9	3,563.56	41.62	10.71	2.33	1.06	2.84	0.07	0.47	19.72	2.55	0.05
N202-11	3,565.25	57.67	13.58	2.39	2.09	2.90	0.13	0.60	4.48	3.88	0.05
N202-13	3,569.90	58.04	15.79	1.81	1.98	3.12	0.12	0.64	3.94	2.73	0.04
N202-14	3,572.43	55.95	13.42	2.47	1.63	3.03	0.12	0.61	7.25	4.65	0.11
N202-15	3,575.35	62.96	11.34	1.61	2.39	2.20	0.11	0.42	6.37	1.94	0.04
G103-1	2,743.60	59.69	14.83	2.53	1.45	2.80	0.10	0.67	5.03	3.74	0.06
G103-2	2,744.80	57.62	15.11	3.03	1.33	2.85	0.10	0.68	5.18	4.16	0.06
G103-4	2,748.30	55.85	16.32	3.01	1.15	3.31	0.15	0.66	3.54	4.87	0.06
G103-5	2,749.80	59.12	12.73	1.95	1.73	2.29	0.09	0.49	7.86	2.99	0.04
G103-6	2,751.80	55.18	15.54	3.26	1.20	2.99	0.11	0.74	5.99	4.14	0.06
G103-7	2,754.10	55.52	16.67	3.49	1.11	3.16	0.10	0.75	4.49	5.25	0.06
G103-8	2,765.30	71.86	11.36	0.69	2.27	1.74	0.06	0.22	3.27	1.44	/

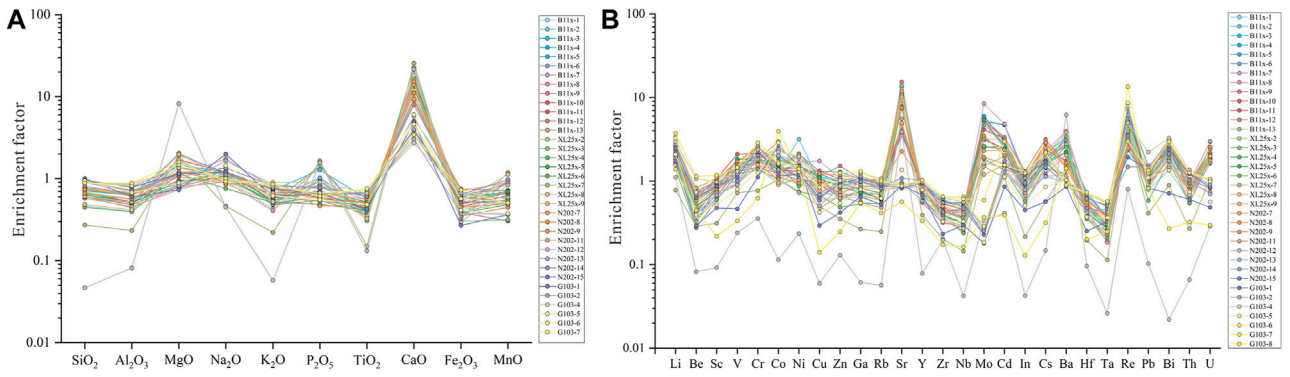

FIGURE 5 | Enrichment factor of the major elements **(A)** (relative to the PAAS, Taylor and Mclennan, 1985) and trace elements **(B)** (relative to the UCC, Taylor and Mclennan, 1985) in the Es_1^L shale.

14.69 wt%, and 11.24 wt%, respectively (**Table 2**). Compared to post-Archaean Australian shale (PAAS) (Taylor and Mclennan, 1985), the CaO, MgO, Na_2O, and P_2O_5 were relatively enriched but the SiO_2, Al_2O_3, Fe_2O_3, MnO, K_2O, and TiO_2 were depleted (**Figure 5A**). The results of the trace element analysis are presented in **Tables 3**, **4**. Compared with the Upper Continental Crust's (UCC) composition (Taylor and Mclennan, 1985), Sr has enrichment factors of 0.57–15.34 (mean 5.60), Mo had enrichment factors of 0.18–8.43 (mean 2.59), Re had enrichment factors of 1.48–13.48 (avg. 4.71), and Ba had enrichment factors of 0.85–3.98 (avg. 2.00).

TABLE 3 | Trace elements results of the Es_1^L shale in the Raoyang Sag.

Samples	Depth (m)	Li (ug/g)	Be (ug/g)	Sc (ug/g)	V (ug/g)	Cr (ug/g)	Co. (ug/g)	Ni (ug/g)	Cu (ug/g)	Zn (ug/g)	Ga (ug/g)	Rb (ug/g)	Sr (ug/g)	Y (ug/g)	Zr (ug/g)
B11x-1	3,397.85	1.66	0.40	0.62	1.03	1.41	0.93	1.08	0.77	0.62	0.57	0.52	13.47	0.58	0.34
B11x-2	3,398.15	2.18	0.45	0.77	1.26	1.77	1.27	3.17	0.96	0.93	0.70	0.65	9.11	0.65	0.43
B11x-3	3,398.95	2.71	0.69	0.96	1.42	2.11	1.42	2.10	1.31	1.28	1.05	0.90	3.52	0.95	0.60
B11x-4	3,410.41	2.02	0.33	0.83	1.80	1.90	1.35	1.53	1.14	0.97	0.77	0.63	4.05	0.77	0.44
B11x-5	3,411.30	2.58	0.77	0.95	1.32	2.09	2.04	1.40	1.22	0.98	0.97	0.82	4.28	0.86	0.58
B11x-6	3,411.65	2.37	0.67	0.84	1.54	1.95	1.97	1.32	0.97	0.92	0.82	0.72	7.41	0.71	0.43
B11x-7	3,412.33	2.52	0.58	1.00	1.78	2.25	2.02	1.67	1.75	1.08	0.97	0.85	8.38	0.88	0.53
B11x-8	3,413.02	1.61	0.34	0.62	1.59	1.56	1.06	1.40	1.05	0.66	0.55	0.48	4.25	0.59	0.42
B11x-9	3,413.93	2.00	0.41	0.67	1.30	1.45	1.25	1.02	0.99	0.71	0.67	0.59	15.34	0.55	0.32
B11x-10	3,414.56	2.23	0.49	0.76	1.42	1.69	1.50	1.10	0.90	0.65	0.75	0.68	4.83	0.72	0.46
B11x-11	3,415.01	2.41	0.62	1.08	2.09	2.17	1.36	1.30	1.33	1.05	0.89	0.83	3.75	0.88	0.49
B11x-12	3,416.17	2.80	0.74	1.01	1.70	2.53	1.51	2.13	1.13	1.51	1.05	1.03	4.43	0.88	0.54
B11x-13	3,417.15	1.72	0.33	0.74	0.91	1.56	1.32	1.12	0.70	0.71	0.67	0.60	13.21	0.79	0.34
Xl25x-2	3,324.89	2.50	0.53	0.95	1.47	2.10	1.41	1.98	1.04	0.92	0.89	0.81	7.78	0.80	0.43
Xl25x-3	3,330.06	1.99	0.50	0.85	1.32	1.85	1.47	0.89	0.89	0.80	0.82	0.71	13.82	0.74	0.42
Xl25x-4	3,331.07	1.81	0.42	0.84	1.55	1.85	1.53	0.87	1.16	0.61	0.75	0.61	10.94	0.89	0.39
Xl25x-5	3,331.99	1.96	0.44	0.80	1.84	1.74	1.79	1.53	1.09	0.84	0.73	0.64	7.40	0.73	0.39
Xl25x-6	3,339.24	1.39	0.28	0.59	1.21	1.38	1.05	0.75	0.67	0.49	0.54	0.54	7.73	0.58	0.38
Xl25x-7	3,340.17	0.78	0.29	0.31	0.72	0.77	1.05	0.73	0.50	0.35	0.27	0.25	5.58	0.39	0.20
Xl25x-8	3,340.67	1.56	0.46	0.74	0.93	1.56	0.90	1.05	0.59	0.63	0.64	0.62	10.20	0.90	0.35
Xl25x-9	3,341.27	2.01	0.66	0.81	1.20	1.83	0.95	1.31	0.77	0.83	0.81	0.80	4.95	0.87	0.51
N202-7	3,560.68	2.69	0.83	1.07	1.70	2.60	1.57	1.92	1.23	1.16	1.10	0.92	2.27	0.96	0.56
N202-8	3,562.31	2.40	0.62	0.90	1.59	2.25	1.38	1.55	1.00	0.89	0.97	1.03	7.48	0.74	0.44
N202-9	3,563.56	2.08	0.59	0.85	1.55	2.05	1.11	0.95	0.90	0.74	0.83	0.91	11.88	0.70	0.40
N202-11	3,565.25	1.88	0.72	0.72	0.92	1.83	2.98	1.25	0.47	0.68	0.98	0.81	0.82	0.86	0.42
N202-13	3,569.90	3.39	0.71	0.68	0.90	1.97	2.35	1.89	0.51	0.85	1.02	0.82	0.96	0.58	0.36
N202-14	3,572.43	1.88	0.73	0.88	1.00	2.04	1.58	1.12	0.60	1.09	0.98	0.87	1.08	1.02	0.43
N202-15	3,575.35	1.73	0.29	0.48	0.47	1.11	2.66	1.50	0.29	0.42	0.65	0.52	0.88	0.68	0.23
G103-1	2,743.60	2.46	0.63	0.86	1.12	2.39	1.16	1.20	0.64	0.93	1.09	0.89	0.83	0.93	0.56
G103-2	2,744.80	2.77	0.70	0.98	1.21	2.58	1.36	1.45	0.69	1.00	1.15	0.93	0.88	0.96	0.55
G103-4	2,748.30	2.99	1.06	0.98	1.30	2.38	2.24	1.97	0.85	0.87	1.24	1.07	0.92	0.99	0.63
G103-5	2,749.80	2.08	0.39	0.52	0.80	1.26	2.89	1.30	0.42	0.54	0.79	0.62	1.36	0.79	0.33
G103-6	2,751.80	3.26	0.74	1.14	1.48	2.88	1.68	1.48	0.85	1.01	1.27	0.98	0.91	0.98	0.65
G103-7	2,754.10	3.73	1.14	1.18	1.45	2.87	1.62	1.41	0.84	1.25	1.31	1.01	0.88	1.02	0.65
G103-8	2,765.30	1.38	0.45	0.22	0.33	0.62	3.92	1.39	0.14	0.25	0.55	0.42	0.57	0.34	0.17

However, Li, Cd, Ni, Co., and Bi showed only minor enrichments or slight depletions (**Figure 5B**). The enrichment or depletion of the above major and trace elements are closely related to changes in the paleosedimentary environment. Therefore, the distribution characteristics of these elements and their paragenetic assemblages can help us construct a connection between the paleosedimentary environment and geochemistry of shale and further reveal the mechanisms of OM input and preservation (He et al., 2017b).

DISCUSSIONS

Paleosedimentary Environment and OM

Clastic Influx Proxies

The providential input of various clastics into ancient lake basins has an impact on the concentration of OM (Ding et al., 2015). The enhanced clastic influx may directly control the enrichment of OM by diluting OM or preventing its burial and preservation (Canfield, 1994).

Areas affected by terrigenous clastics have relatively high Fe_2O_3+Al_2O_3 contents, and areas dominated by biochemical performance have relatively high CaO + MgO contents. The value of (Fe_2O_3+Al_2O_3)/(CaO + MgO) reflects the relative strength of terrigenous clastic sedimentation and biochemical sedimentation in lake basins (Zhou et al., 2020). When the supply of terrigenous clastics increases, Fe_2O_3 and Al_2O_3 content increases, and when the capacity of terrigenous clastics is weakened and biochemical deposition is enhanced, CaO and MgO content will increase. On the plane, the migration ability of Fe_2O_3 and Al_2O_3 was weak, and the migration ability of CaO and MgO was stronger (Xu et al., 2007). Their ratios were thus high at provenance and gradually declined as the distances from the provenance increased (Zhou et al., 2020). When (Fe_2O_3+Al_2O_3)/(CaO + MgO) > 1, the sediment is mainly controlled by terrigenous clastics; when (Fe_2O_3+Al_2O_3)/(CaO + MgO) < 1, it is mainly a biochemical deposition; and when (Fe_2O_3+Al_2O_3)/(CaO + MgO) is in the range of 0.5–1.0, it is in a transitional state, which is jointly controlled by terrigenous clastics and biochemical deposition in the lake basin. In the samples from the four key wells in the study area, the values of (Fe_2O_3+Al_2O_3)/(CaO + MgO) were 0.50 (Xl25x), 0.76 (B11x), 1.71 (N202), and 2.54 (G103). The shale of wells G103 and N202 was obviously determined by terrigenous clastics, which is consistent with the

TABLE 4 | Trace elements results of the Es_1^L shale in the Raoyang Sag.

Samples	Depth (m)	Nb (ug/g)	Mo (ug/g)	Cd (ug/g)	In (ug/g)	Cs (ug/g)	Ba (ug/g)	Hf (ug/g)	Ta (ug/g)	Re (ug/g)	Pb (ug/g)	Bi (ug/g)	Th (ug/g)	U (ug/g)
B11x-1	3,397.85	0.26	2.53	2.42	0.53	1.34	3.35	0.37	0.19	3.99	0.79	1.34	0.56	1.63
B11x-2	3,398.15	0.35	3.11	2.46	0.85	1.74	2.85	0.46	0.25	4.20	0.93	1.78	0.68	2.07
B11x-3	3,398.95	0.51	5.18	4.69	1.21	2.16	3.31	0.68	0.38	6.98	1.52	2.54	1.04	1.91
B11x-4	3,410.41	0.36	5.99	2.97	0.79	1.57	2.23	0.48	0.27	2.35	1.05	2.22	0.81	2.12
B11x-5	3,411.30	0.49	5.25	4.73	1.09	2.01	2.61	0.73	0.37	5.91	1.27	2.61	0.97	2.96
B11x-6	3,411.65	0.36	4.71	2.80	1.02	1.92	3.05	0.49	0.29	6.83	1.10	2.29	0.83	2.09
B11x-7	3,412.33	0.45	8.43	4.83	1.23	2.28	3.98	0.63	0.36	7.10	1.45	3.11	0.97	3.00
B11x-8	3,413.02	0.24	5.18	2.46	0.61	1.20	2.07	0.45	0.18	3.16	0.89	2.00	0.57	1.68
B11x-9	3,413.93	0.28	5.26	3.21	0.76	1.70	2.85	0.38	0.22	2.76	0.85	1.87	0.67	1.89
B11x-10	3,414.56	0.35	3.21	2.40	0.77	1.93	2.58	0.53	0.28	5.41	0.95	1.83	0.76	1.85
B11x-11	3,415.01	0.36	4.12	3.21	0.96	2.35	1.75	0.56	0.29	2.89	1.07	2.46	0.88	1.83
B11x-12	3,416.17	0.46	5.50	3.35	1.31	3.16	1.62	0.58	0.38	4.79	1.30	3.12	1.04	2.02
B11x-13	3,417.15	0.29	1.54	1.96	0.78	1.58	2.56	0.35	0.25	3.15	0.83	2.08	0.66	1.64
Xl25x-2	3,324.89	0.39	3.24	3.11	0.91	2.24	2.74	0.48	0.31	4.17	1.00	2.37	0.87	2.18
Xl25x-3	3,330.06	0.36	2.57	2.58	0.96	1.98	2.54	0.46	0.31	4.69	0.89	2.32	0.85	2.11
Xl25x-4	3,331.07	0.30	2.62	2.41	0.71	1.62	3.40	0.41	0.27	3.50	1.03	2.56	0.72	1.77
Xl25x-5	3,331.99	0.32	5.40	2.60	0.92	1.73	2.20	0.41	0.27	5.55	1.12	2.98	0.76	2.52
Xl25x-6	3,339.24	0.24	1.84	1.35	0.57	1.44	1.22	0.36	0.21	3.90	0.58	1.70	0.54	2.04
Xl25x-7	3,340.17	0.14	1.49	1.10	0.22	0.57	1.37	0.19	0.11	3.97	0.41	0.89	0.27	1.06
Xl25x-8	3,340.67	0.27	1.65	1.44	0.68	1.45	2.03	0.37	0.24	3.57	0.82	1.85	0.68	1.96
Xl25x-9	3,341.27	0.40	1.20	1.55	0.96	2.06	3.82	0.54	0.33	5.09	0.99	1.77	0.80	1.98
N202-7	3,560.68	0.50	2.30	2.36	1.18	2.49	1.56	0.60	0.40	2.49	1.30	3.04	1.03	1.76
N202-8	3,562.31	0.46	3.46	2.04	1.16	2.79	1.44	0.51	0.38	3.25	1.19	2.90	0.93	2.41
N202-9	3,563.56	0.43	1.93	1.60	0.97	2.88	1.65	0.46	0.34	2.86	0.99	2.63	0.79	2.55
N202-11	3,565.25	0.46	0.23	1.26	0.72	1.14	1.17	0.44	0.46	8.50	1.03	1.48	0.96	0.74
N202-13	3,569.90	0.48	0.26	1.31	0.79	1.13	0.97	0.42	0.47	6.17	1.53	1.74	1.00	0.70
N202-14	3,572.43	0.47	0.23	1.74	0.95	1.46	0.94	0.48	0.43	3.49	1.06	2.12	1.03	0.82
N202-15	3,575.35	0.30	0.18	0.86	0.45	0.57	0.85	0.25	0.33	7.49	0.82	0.71	0.60	0.49
G103-1	2,743.60	0.54	0.23	1.52	1.16	1.70	0.96	0.63	0.50	1.94	1.35	2.38	1.21	0.84
G103-2	2,744.80	0.56	0.27	1.41	1.08	1.91	1.03	0.62	0.51	1.48	1.46	2.70	1.24	0.90
G103-4	2,748.30	0.56	0.29	1.12	1.30	2.17	1.01	0.70	0.55	4.96	2.23	3.27	1.36	1.01
G103-5	2,749.80	0.33	0.18	1.12	0.51	0.85	1.03	0.37	0.37	8.62	1.10	1.35	0.74	0.56
G103-6	2,751.80	0.65	0.29	1.55	1.28	2.12	0.88	0.71	0.56	3.08	1.25	3.03	1.26	1.06
G103-7	2,754.10	0.61	0.59	2.98	1.25	2.20	0.90	0.73	0.57	2.97	1.35	2.94	1.26	0.99
G103-8	2,765.30	0.16	0.37	0.39	0.13	0.32	1.42	0.20	0.25	13.48	0.82	0.27	0.32	0.30

accepted source direction of Raoyang Sag (Yin et al., 2020). Well B11x was in a transitional state, and well Xl25x was mainly controlled by biochemical deposition. The input intensity of terrigenous clastics was negatively correlated with the TOC value (**Figure 6A**). When $(Fe_2O_3+Al_2O_3)/(CaO + MgO) > 1$, the TOC content is low overall. The samples from wells G103 and N202 were close to the provenance, the input intensity of terrigenous clastics was strong, and the OM was not enriched, due to dilution. Wells B11x and Xl25x were far away from the provenance, and the OM presented different degrees of enrichment. Therefore, the dilution effect of clastic influx impacts the preservation of OM; however, the correlation is not high, indicating that this factor is not the main controlling factor. Moreover, elements such as Ti, Si, and Al are considered to be parameters that can characterize the input intensity of terrigenous clastics (Murphy et al., 2000). Ti is usually associated with clay minerals and heavy minerals, whereas Si mainly exists in quartz, feldspar, and biogenic fractions (Kidder et al., 2001). The elements Ti and Si can provide key information about the variation in the imported flux of clastics from non-aluminosilicate sources after normalizing Al (Chen et al., 2016). The sample concentrations of Ti, Si, and Al from wells G103 and N202 were generally high, while the concentrations from wells B11x and Xl25x were generally low. This shows that different well positions on the plane are affected by the intensity of the clastic influx, which supports the previous discussion. The strong correlations between Ti and Al ($R^2 = 0.85$) and Si and Al ($R^2 = 0.69$) (**Figures 6B,C**) suggest a rather homogeneous detrital supply.

Paleoclimate Proxies

The paleoclimate in provenantial terrain determined the mineralogical and chemical composition of siliceous clastic sediments (Nesbitt and Young, 1982; Fedo et al., 1995). Therefore, the characteristics of mineralogical and chemical compositions in shale can potentially reflect changes in paleoclimate. Correspondingly, paleoclimatic conditions can be inferred from the discrimination charts of various elements (CIA, K_2O/Al_2O_3, Ga/Rb, and Rb/Sr) (Fedo et al., 1995; Shen et al., 2001; Roy and Roser, 2013).

The chemical index of alteration (CIA) can aid in the reconstruction of paleoclimate and weathering intensity (Fedo et al., 1995; Price and Velbel, 2003), and the CIA equation can be expressed as $[(Al_2O_3)/(Al_2O_3 + Na_2O+ CaO^* + K_2O)] \times 100)$. As it is unclear whether CaO is derived from carbonate, Nesbitt and

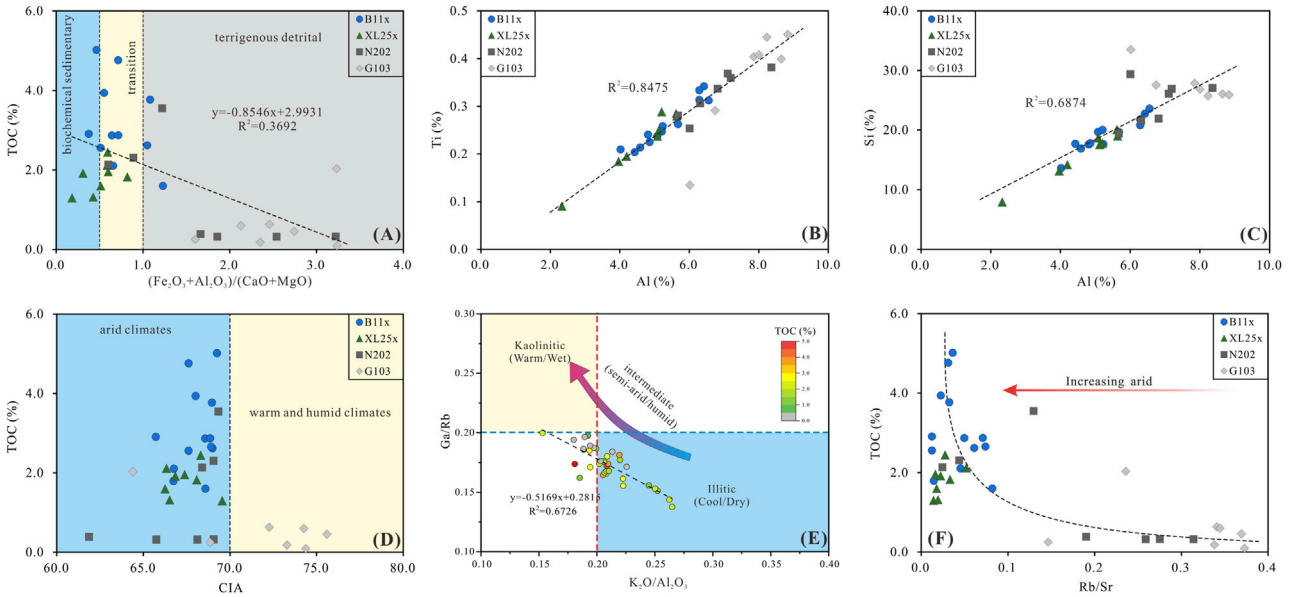

FIGURE 6 | Provenance and paleoclimate analysis of Es_1^L shale.

Young (1984) suggested excluding CaO from CIA calculations on rocks with high CaO content. As mentioned in *Mineralogy and Lithofacies of Shale*, the Es_1^L shale is rich in carbonate, and the corrected CaO content is much greater than the Na_2O content; therefore, CaO* should be replaced by Na_2O in the CIA formula. When CIA values are high (85–100), sediments were generally deposited in hot and humid tropical paleoclimates, whereas those deposited in warm and humid paleoclimates have medium CIA values (70–85), and those deposited in cold and arid paleoclimates have minor CIA values (50–70) (Nesbitt and Young, 1982). In this study, the CIA values of shale from Es_1^L varied from 62 to 76 (mean 68), and only five samples from well G103 had values greater than 70 (**Figure 6D**), indicating that the sediments were produced in the source region, under a cold and arid paleoclimate. In addition, the Es_1^L shale seems to have been deposited in arid to semi-arid paleoclimate conditions, according to the Ga/Rb and K_2O/Al_2O_3 discriminant chart (**Figure 6E**), which is consistent with the results obtained by Ye et al. (2020). The value of Rb/Sr can also indicate the evolution of the paleoclimate. Element Rb is relatively stable, whereas Sr is easily weathered during chemical weathering. Therefore, Rb/Sr values are high in humid environments and relatively low in dry and hot environments (Shen et al., 2001; Li et al., 2019; Ye et al., 2020). The Rb/Sr values of all samples from well G103 and some of those from well N202, located at the boundary of the Raoyang Sag, were larger, while the Rb/Sr values of wells B11x and Xl25x, located in the middle of the sag, were relatively small (**Figure 6F**). In addition, it was observed that the TOC content increased with aridity (**Figure 6F**). The mineral composition of sediments can also reflect climatic change. Carbonates are deposited under dry climatic conditions because of the elevated evaporation (Kelts and Hsu, 1978; Sarnthein et al., 1994). Therefore, the degree of arid climate in Es_1^L may increase the salinity of lakes, deposition of carbonates, and eutrophication in lake waters, resulting in algal blooms and OM enrichment. Therefore, climate has an impact on the accumulation of OM and is also a condition for the formation of basins with small areas but large resources.

Paleoredox Conditions Proxies

The paleoredox conditions of ancient lakes play a vital role in the deposition, burial, preservation, and accumulation of OM. Such conditions can usually be characterized by specific ratios of redox-sensitive elements (e.g., Th/U, V/(V + Ni), Ni/Co., and V/Cr) (Hatch and Leventhal, 1992; Jones and Manning, 1994; Wignall and Twitchett, 1996; Rimmer et al., 2004), which include Mo, U, Th, V, Ni, Co., and Cr (Zhao et al., 2016; He et al., 2017b). However, some of the specific trace elements (e.g., Cr and Co.) found in lacustrine sedimentary rocks are easily influenced by clastic influx, diagenesis, and re-oxidization after deposition (Xiong et al., 2010). Therefore, the observed ratios of some redox-sensitive elements (e.g., V/Cr and Ni/Co.) may result in misinterpretations and are no longer considered suitable for accurately reflecting paleoredox conditions.

In this study, the V/(V + Ni) values of the Es_1^L shale were between 0.42 and 0.84 (avg. 0.72). Most of the V/(V + Ni) ratios in shale samples exceeded the threshold values (i.e., V/(V + Ni) > 0.6) indicative of dysoxic/suboxic conditions (**Figure 7A**), which demonstrates that the Es_1^L shales were mainly deposited in a dysoxic/suboxic paleo-lacustrine environment. Under decreasing water conditions, organic-rich sediments are rich in U (Kochenov et al., 1977). Thus, low Th/U ratios have been widely used as indicators of anoxic paleo-sedimentary environments (Th/U < 2) (Wignall and Twitchett, 1996). The Th/U values of the shale samples were widely distributed across the range of 0.97–5.53 (mean 2.56), indicating the paleoredox conditions of ancient lake are inconsistent and there are differences in the vertical

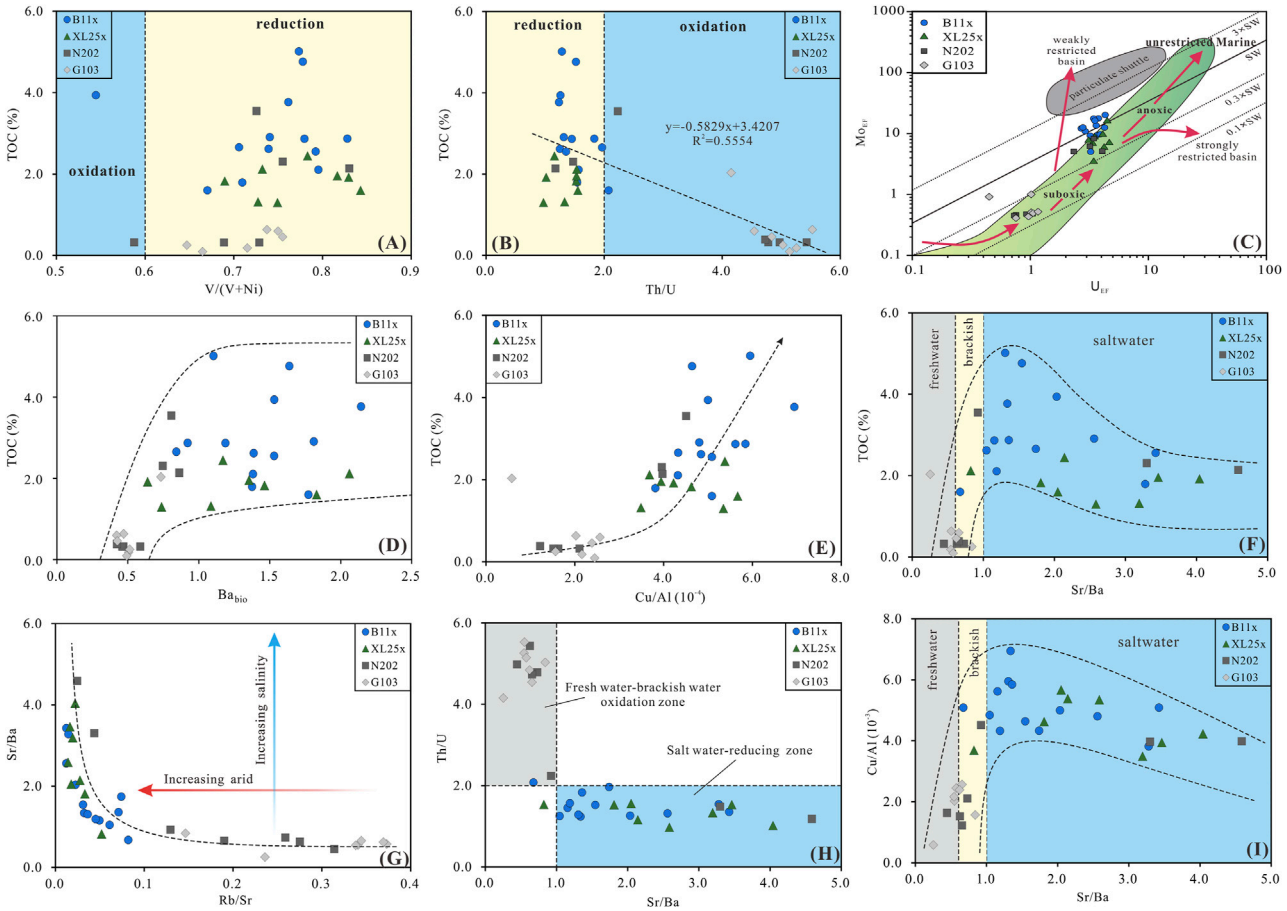

FIGURE 7 | Analysis of paleoredox conditions, paleoproductivity, and paleosalinity.

preservation conditions. The Th/U ratios of organic-rich shale (>1.7%) were usually less than 2 (mean 1.59), which indicates that these shale samples were deposited in a reducing paleoenvironment. Moreover, the TOC and Th/U ratios have a strong negative correlation (R^2 = 0.55) (**Figure 7B**). These observations show that paleoredox conditions, that is, preservation conditions, played a major role in controlling the enrichment of OM in the Es_1^L shale.

U and Mo are also effective paleoredox parameters that are disturbed by external factors and can accurately reflect the occurrence of paleoredox conditions during sediment deposition processes (Tribovillard et al., 2006). Previous research has shown that the patterns of U_{EF}-Mo_{EF} covariations are particularly significant for paleoredox reconstruction (Algeo and Tribovillard, 2009; Wang et al., 2017). U_{EF} and Mo_{EF} represent the element enrichment factors (MEFs) of U and Mo, respectively. The calculation formula for M_{EF} is:

$$M_{EF} = (X/Al)_{sample}/(X/Al)_{PASS} \quad (1)$$

where X and Al are the concentrations of elements X and Al, respectively. Mo and U showed obvious enrichment in wells B11x, Xl25x and in some of the samples from N202; whereas the elements Mo and U from the G103 well and some of the samples from the N202 well exhibited relatively moderate or less detectable enrichment (**Figure 7C**). These parameters indicate that the shale samples from wells B11x and Xl25x and some from N202 were possibly deposited in a water column with abundant H_2S, whereas the samples from well G103 and others from N202 were deposited in water with scarce H_2S (Algeo and Tribovillard, 2009; Wang et al., 2017). The semi-deep and deep lake had a reducing paleoenvironment, whereas the shallow lake sediments reflected oxic and suboxic paleoenvironments, based on the plot of the Mo_{EF}-U_{EF} covariation and sedimentary facies belt for each well location (**Figure 7C**).

Paleoproductivity Proxies

Elemental Ba and Cu can depict relative levels of paleoproductivity (Tribovillard et al., 2006). Their correlation with TOC is usually used as a proxy for the impact of primary productivity on OM enrichment (Zhao et al., 2016; Wang et al., 2017), based on the premise that OM is produced by algae (primary productivity) (Pedersen and Calvert, 1990). Indeed, previous research has determined that algae organisms are the main origin of OM in the Es_1^L source rock (Yin et al., 2020).

Therefore, paleoproductivity proxies are valuable for evaluating OM enrichment.

Barium is considered a typical index for evaluating paleoproductivity because biogenic barite is associated with phytoplankton decay (Dymond et al., 1992). Biogenic Ba (Ba_{bio}) can be used to estimate the intensity of carbon exports from the photic zone in the water column and is regarded as an effective indicator of paleoproductivity (Brumsack, 1989; Tribovillard et al., 1996). The Ba_{bio} content can be obtained using the following formula:

$$Ba_{bio} = Ba_{tot} - (Al_{tot} \times Ba / Al_{alu}) = Ba_{tot} - (Al_{tot} \times 0.0075) \quad (2)$$

where Ba_{bio} is the Ba content from the biogenic component, Ba_{tot} is the total Ba content, Ba/Al_{alu} is the Ba/Al ratio of aluminosilicate detritus in crustal rocks, and Al_{tot} is the total Al content. The Ba/Al_{alu} ratios of aluminosilicate components in crustal rocks ranged from 0.005 to 0.01 (Taylor, 1964) and the Ba/Al_{alu} ratios usually had a value of 0.0075 (Dymond et al., 1992). The Ba_{bio} contents of the samples from different regions were quite different. The samples from semi-deep lacustrine and deep lacustrine facies had higher Ba_{bio} content, whereas the Ba_{bio} content in samples from shore-shallow lake facies was relatively low. The abundance of TOC is directly related to paleoproductivity, and TOC is more abundant when Ba_{bio} content is greater than 1.0 (**Figure 7D**). Therefore, paleoproductivity is of great significance for the enrichment of OM.

OM incorporates copper (Cu) into sediments in the form of organometallic complexes, so there is a close relationship between Cu and TOC content (Tribovillard et al., 2006). Therefore, while OM may become partially or completely degraded after deposition, the Cu released from OM can be trapped by pyrite and preserved in sediment (Huerta-Diaz and Morse, 1992; Algeo and Maynard, 2004). Thus, the ratio of Cu to Al can represent the level of paleoproductivity (Tribovillard et al., 2006). The average value of Cu/Al in the shale samples was 3.86×10^{-3}, and the Cu/Al values of samples from wells B11x and Xl25x and some from N202 were much higher than those from G103 and others from N202 (**Figure 7E**). The samples from shore-shallow lake facies implied relatively low paleoproductivity, which may be due to the destruction of the phytoplankton growth environment by clastic influx. In addition, the concurrence of increased TOC content and Cu/Al (**Figure 7E**) indicates that paleoproductivity has an impact on OM enrichment.

Paleosalinity Proxies

The chemical properties of Sr and Ba are similar, and the migration ability of Ba is lower than that of Sr, so Sr can continue to migrate further towards, or away from, areas of higher salinity. Thus, Sr/Ba ratios usually indirectly indicate the salinity of the water body (Fu et al., 2018; Zhou et al., 2020). According to previous research, water can be classified as a freshwater (Sr/Ba<0.6), brackish (0.6<Sr/Ba<1.0), or saline environment (Sr/Ba>1.0) (Wang et al., 1979; Wang and Wu, 1983). The average Sr/Ba values of wells B11x, Xl25x, N202, and G103 were 1.74, 2.51, 1.61, and 0.58, respectively; indicating that the first three wells experienced saline environmental conditions, while well G103 experienced a freshwater environment. The average depths of the sampling points of the above four wells were 3,410.04, 3,336.08, 3,567.07, and 2,751.10 m, respectively, which corresponds to their historical salinity conditions. These observations demonstrate that the semi-deep and deep lake water bodies had relatively high salinities and were vertically heterogeneous with stratified water columns.

The TOC content first increased and then decreased with increases in paleosalinity (**Figure 7F**). TOC was more enriched when the value of Sr/Ba was 1.0–3.0, indicating that both low paleosalinity and excessive paleosalinity were not conducive to the enrichment of OM, which is consistent with the results of He et al. (2018); based on their use of biomarker compounds in paleosalinity analysis.

We also found that arid climates caused evaporation to significantly reduce lake water levels, which increased the salinity of the deep lake water body (**Figure 7G**). However, the shallow lake area was more affected by the influx of terrestrial debris and experienced a high turnover of water exchange, resulting in low salinity and water column stratification. Saltwater environments in the study area also usually experienced reducing conditions, with freshwater and brackish water having oxidizing conditions [**Figures 7H**, **8** (profile 1 in **Figure 1A**)]. This indicates that water column stratification also induced different preservation conditions at different lake depths. This is also confirmed by the extensive development of laminar structures (**Figures 4B,H,J**). In addition, the productivity profile (Cu/Al) also exhibited a phenomenon in which it first increased and then decreased with increasing salinity, indicating that neither freshwater nor excessive salinity were suitable environments for ancient organisms (algae, etc.) (**Figure 7I**). Therefore, salinity is important for OM enrichment. The low input of terrestrial debris, arid climate, moderate lake salinity, reducing environment, and high productivity are conducive to OM enrichment.

OM and Shale Oil Enrichment

The first two geochemical indices that can directly reflect the oil content within shale are the amounts of chloroform bitumen S_1 and "A" (Lu et al., 2012). The former represents low-carbon hydrocarbon content, and the latter is the sum of heavier hydrocarbons, nonhydrocarbons, and asphaltenes (Li et al., 2015). The S_1 of shale samples can be used as an indicator to evaluate absolute oil content because most shale reservoirs have low permeability and produce light or condensate oil.

Figure 9A illustrates the relationship between the oil content and TOC of shale samples from Es_1^L. The oil content of the samples exhibits the characteristics of a triple-division with increases in TOC value. First, the oil content of the samples increased slowly when the TOC was low, then rose rapidly for a while, finally entering a steady state. According to the absolute oil content corresponding to the turning points of the envelope of the scattered points in **Figure 9A**, the shale samples were classified into three types, based on the TOC value of the turning points: dispersed resources (TOC < 0.6%), potential resources (0.6% <TOC<1.7%), and enriched resources (TOC > 1.7%). Enriched resources mean that the total oil generated by the OM can meet

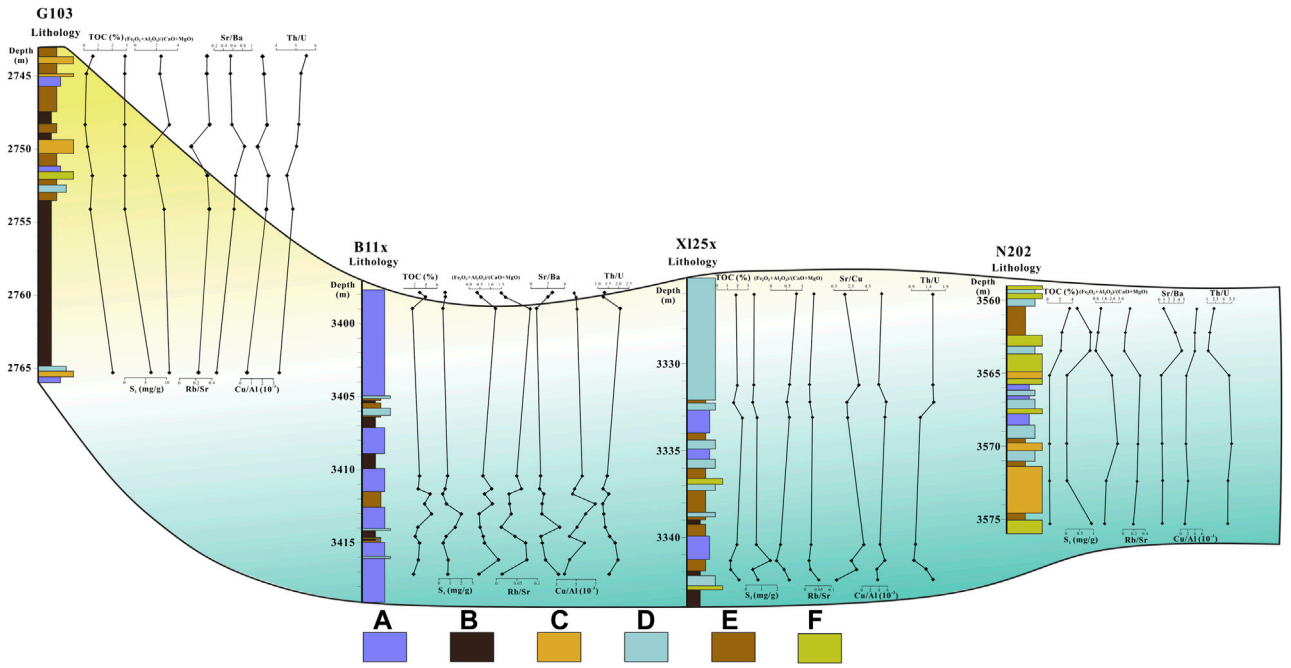

FIGURE 8 | Paleoenvironment conditions from sections of the wells.

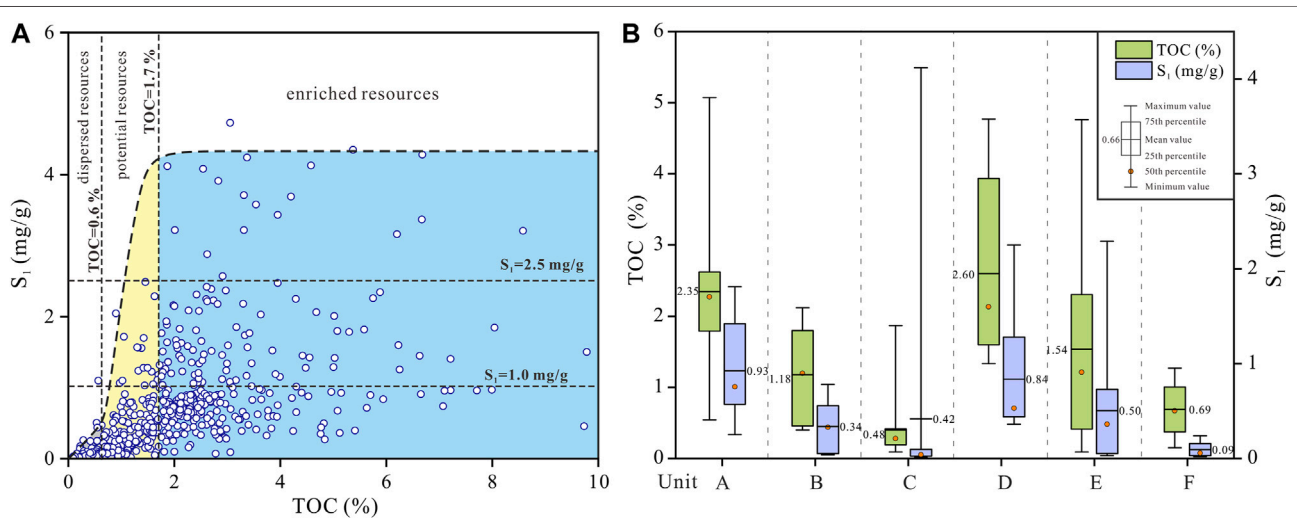

FIGURE 9 | (A) Relationship between S_1 and TOC in Raoyang Sag **(B)** Comparison of organic geochemical parameters of different lithofacies (A: Carbonate-rich shale; B: Clay-rich shale; C: Felsic-rich shale; D: Calcareous shale; E: Clay shale; F: Felsic shale).

the requirements of shale residual oil when the TOC reaches a critical value (1.7%). The hydrocarbons in shales are saturated, resulting in their expulsion when the TOC exceeds the critical value (Lu et al., 2012). The layer formations with enriched resource conditions are the most promising exploration targets for shale oil. In addition, the OM and hydrocarbon enrichment of different lithofacies also varied (**Figure 9B**). Types A, D, and E of OM were more enriched (mean values were 2.35, 2.60, and 1.54, respectively) and corresponded to enriched resources. The characteristics of self-generation and self-storage of shale oil also enriched the hydrocarbons of Types A, D, and E (mean values were 0.93, 0.84, and 0.50, respectively). This shows that carbonate minerals play an important role in shale oil enrichment. Previous studies have shown that the mesopores and macropores (dissolution pores, intercrystalline pores and microfractures) existing in the lacustrine shale interval are closely

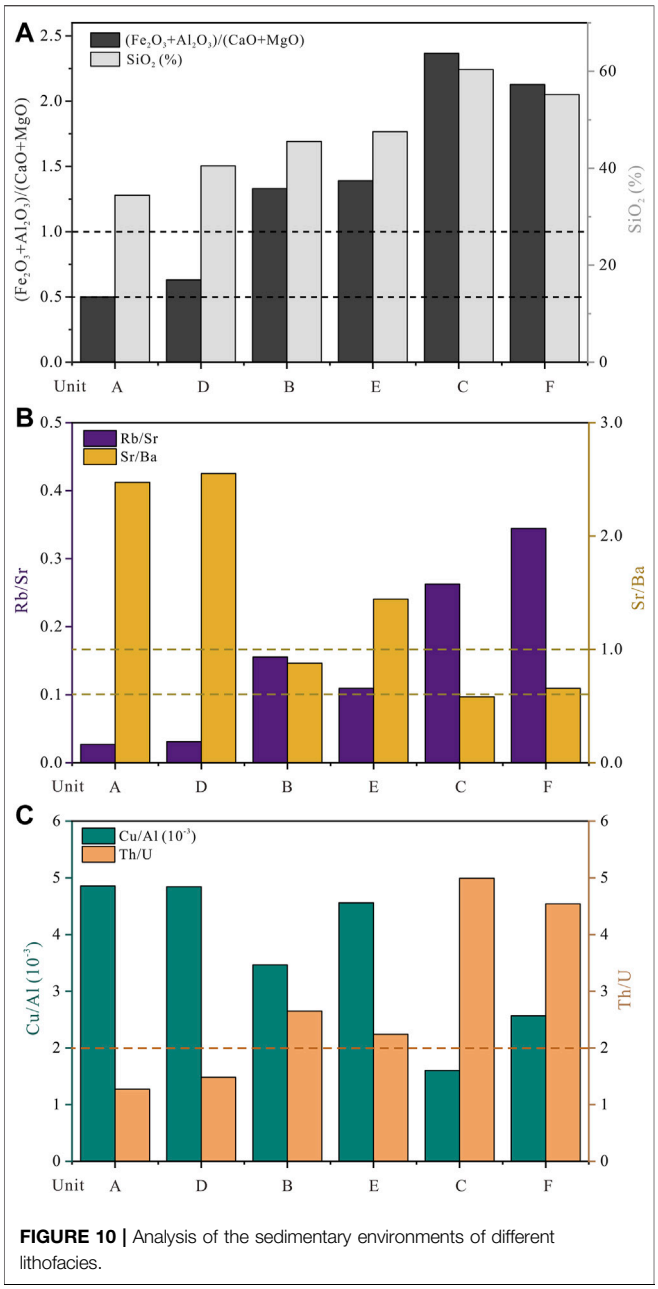

FIGURE 10 | Analysis of the sedimentary environments of different lithofacies.

related to the carbonate composition, which is a key factor affecting the quality of the shale oil reservoir. Moreover, larger pores are most conducive to the enrichment and development of shale oil (Wang et al., 2015; Birdwell et al., 2016; Li et al., 2017; Bai et al., 2020). It is worth noting that there were abnormally high values of Type C, which may have been caused by the migration of hydrocarbons in the surrounding organic-rich shale. For shale oil reservoirs with mainly self-generation and self-storage characteristics, OM content is a cornerstone that largely determines the degree of hydrocarbon enrichment in shale. The different types of shale have varying degrees of OM enrichment because of their dissimilar sedimentary environments.

Paleosedimentary Environment and Lithofacies

The deposition period of A and D was less affected by terrigenous clastic input ($(Fe_2O_3+Al_2O_3)/(CaO + MgO) < 1.0$), and TOC was rarely diluted. The paleoclimatic conditions corresponding to the two lithofacies were relatively arid, leading to increased lake concentration, moderate paleosalinity (1.0<Sr/Ba<3.0), and a massive precipitation of calcareous minerals. A favorable paleoclimatic environment and moderate paleosalinity provided a good habitat for algae and other organisms, causing them to flourish in large numbers, resulting in a significant increase in paleoproductivity. The OM formed by paleontology deposited in stratified water columns, and the strong reducing conditions (Th/U < 2.0) guaranteed the enrichment of the OM (**Figure 10**). Organic-rich shale (e.g., A and D) produced hydrocarbons in large quantities and accumulated *in situ* to form shale oil reservoirs under the changing formation temperature and pressure conditions caused by an increase in burial depth.

Types C and F are quite different from the above two lithofacies. They were greatly affected by the input of terrestrial debris—silicon content was relatively high ($SiO_2 > 50\%$), and the OM was severely diluted. During the period of deposition, they experienced a humid paleoclimate, frequent water body exchanges, and low lake water paleosalinity (Sr/Ba < 0.6). These conditions meant that the water bodies were generally rich in oxygen and had low paleoproductivity, resulting in low OM generation, preservation, and enrichment (**Figure 10**). Although lithofacies C and F have low OM contents and lack the capacity to generate a large number of hydrocarbons because of the large amount of felsic minerals trapped by organic-rich shale, their high-quality storage capacity should be noted (**Figure 9B**).

After terrigenous detrital material was brought into the lake basin, fine-grained clay in the water body was concentrated in a suspended state. When suspension equilibrium conditions were broken, the fine-grained clay was gradually deposited in the form of single particles mixed with felsic minerals, carbonates, OM, and other components to form clay shale. The lithological compositions of B and E are mainly clay minerals and were deposited in a sedimentary environment that was not strongly affected by terrigenous clastics and was partial to reduction and brackish water-saltwater bodies (**Figure 10**).

Enrichment Model of Shale Oil

We used a BP neural network combined with logging data and measured XRD data (Li et al., 2015) to predict the rock mineral composition of 79 wells in the study area. The lithofacies profile of N201-N301 was obtained, as shown in **Figure 11**, corresponding to profile 2 in **Figure 1A**. The shale oil enrichment model of the Raoyang Sag, which takes lithofacies and sedimentary environments into account, has been established.

The overall mineral composition of the Raoyang Sag changes from felsic minerals to clay and carbonate and back to felsic minerals, from northwest to southeast, reflecting changes in the sedimentary environment. Under a background of arid paleoclimate, rainfall decreased, weathering and denudation of source rock areas weakened, and the detrital material transported by the river decreased. Because lake water evaporation was greater

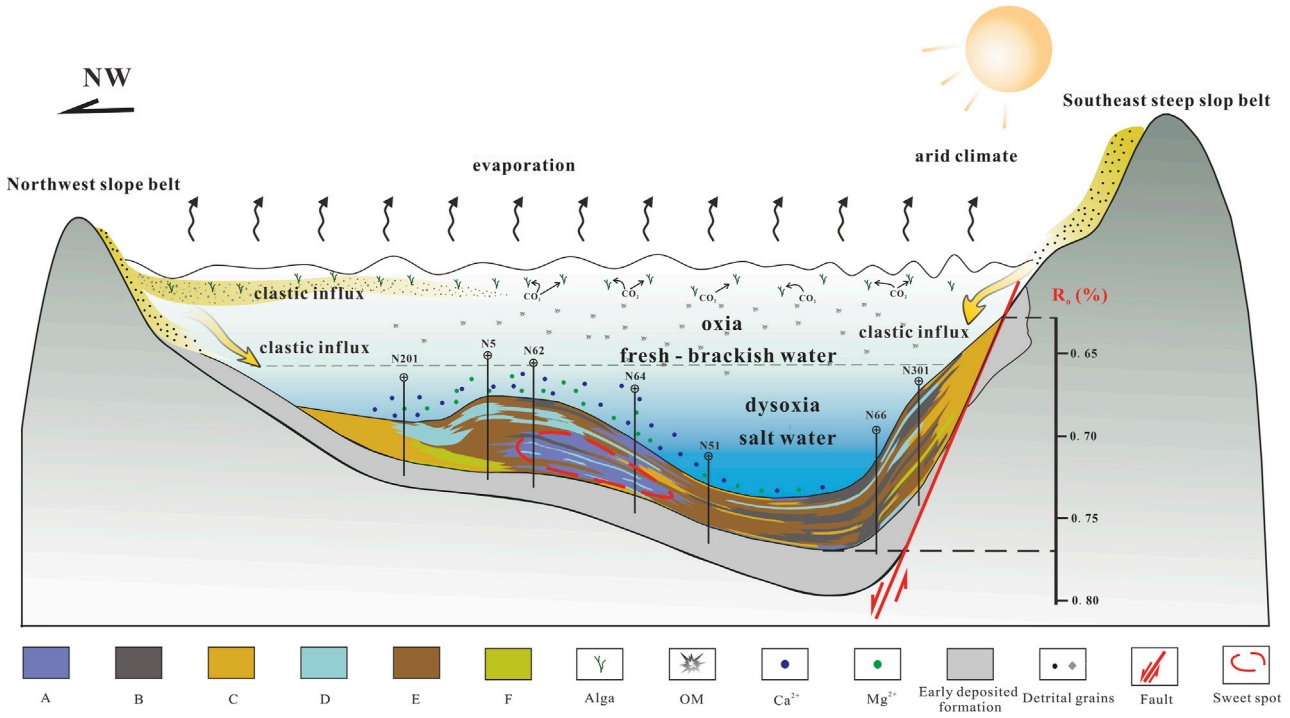

FIGURE 11 | Accumulation model of shale oil in the Es_1^L of the Raoyang Sag.

than the inflow, the lake level entered a downward cycle, the concentration of Ca^{2+} and Mg^{2+} in the lake water gradually increased, and the lake basin entered a salty period. Under appropriate lake water salinity, algae bloomed and consumed the CO_2 in the water body, and a large amount of OM was deposited in the stratified water column. Good storage conditions (strongly reducing) and an environment far from the material source provided conditions for OM enrichment. OM and the seasonal deposition of carbonate rocks deposited under biological and chemical sedimentation formed organic-rich calcareous shale, which is a favorable source reservoir for shale oil. A large volume of terrigenous debris was imported, and the water body was relatively turbulent, which can be attributed to the shallow water high-energy oxidation environment in the slope belt and steep slope belt of the Raoyang Sag. Most of the provenantial felsic minerals entered the lake directly to form C and F near their provenance. Externally sourced fine-grained clay minerals were dispersed and suspended in the lake water, and they were mixed with felsic minerals, carbonates and adsorbed OM deposited in semi-deep and deep lake regions.

Because the lithofacies of A and D were mostly formed in a depositional environment with low debris influx, an arid paleoclimate, moderate paleosalinity, high paleoproductivity, and good preservation conditions, the OM was abundantly enriched. With the increase in stratum burial depth, the OM generated hydrocarbons to form self-generated and self-stored *in situ* shale oil reservoirs (sweet spots) (**Figure 11**). Although clay minerals usually carry OM and are deposited on the bottom of lakes, this type of shale oil reservoir has low movable oil content and generally poor development characteristics due to the strong adsorption and poor fracturing properties of clay minerals (Ju et al., 2018; Li et al., 2018). In addition, the C and F types of lithofacies sandwiched by mature organic-rich shale might also have been enriched oil due to the short-distance migration of hydrocarbons from the organic-rich shale.

CONCLUSION

In this study, the reconstruction of the paleoenvironment of the Es_1^L shale in the Raoyang Sag was based on geochemical, mineralogical, and well logging data, and was used to establish an enrichment model of OM and shale oil that corresponds to the paleosedimentary environment.

The shale oil enrichment model of the Es_1^L in Raoyang Sag was established through a combination of lithofacies and paleosedimentary environments. The kerogen type of the Es_1^L shale is mainly Type I. The shales are also rich in carbonate minerals, with an obvious enrichment of major elements (e.g., CaO, MgO, and Na_2O) and trace elements (e.g., Sr, Mo, and Re). These elements reflect the relationship between the specific paleosedimentary environment and OM. The parameters $(Fe_2O_3+Al_2O_3)/(CaO + MgO)$, Sr/Ba, Rb/Sr, Cu/Al, and Th/U indicate that the Es_1^L shale in the Raoyang Sag was deposited under an arid paleoclimate, reducing conditions, and a paleoenvironment dominated by saline water. OM accumulation in the shale was mainly controlled by the high paleoproductivity of surface water from algal blooming and moderate salinity, with the help of a stratified water column under strong reducing water

conditions. The influx of clastics had a significant effect on the OM. Carbonate plays an important role in shale oil enrichment, and class A and D shales are the dominant lithofacies for shale oil and OM enrichment. Owing to deposition occurring in an arid paleoclimate, conducive salinity water bodies, high paleoproductivity, lower clastic influx, and anoxic preservation conditions were beneficial for OM and shale oil enrichment.

DATA AVAILABILITY STATEMENT

The raw data supporting the conclusion of this article will be made available by the authors, without undue reservation.

AUTHOR CONTRIBUTIONS

YW and ZS collected the samples. YQ, TJ, and YG prepared the samples. YW and ZS completed part of the experimental test. XyL, RZ, XdL, TJ, TZ, and MZ provided some data. YW and SL conceived the project, analyzed the samples, and wrote the manuscript. All authors reviewed the manuscript.

FUNDING

This work was supported by the National Natural Science Foundation (Grant Nos. 41972123 and 41922015).

REFERENCES

Algeo, T. J., and Maynard, J. B. (2004). Trace-element Behavior and Redox Facies in Core Shales of Upper Pennsylvanian Kansas-type Cyclothems. *Chem. Geology.* 206, 289–318. doi:10.1016/j.chemgeo.2003.12.009

Algeo, T. J., and Tribovillard, N. (2009). Environmental Analysis of Paleoceanographic Systems Based on Molybdenum-Uranium Covariation. *Chem. Geology.* 268, 211–225. doi:10.1016/j.chemgeo.2009.09.001

Bai, C., Yu, B., Han, S., and Shen, Z. (2020). Characterization of Lithofacies in Shale Oil Reservoirs of a Lacustrine basin in Eastern China: Implications for Oil Accumulation. *J. Pet. Sci. Eng.* 195, 107907. doi:10.1016/j.petrol.2020.107907

Birdwell, J. E., Berg, M., Johnson, R. C., Mercier, T. J., Boehlke, A. R., and Brownfield, M. D. (2016). *Geological, Geochemical and Reservoir Characterization of the Uteland Butte Member of the Green River Formation*. Utah: Uinta Basin.

Brumsack, H.-J. (1989). Geochemistry of Recent TOC-Rich Sediments from the Gulf of California and the Black Sea. *GEOL. RUNDSCH* 78, 851–882. doi:10.1007/bf01829327

Cai, Y., Liu, D., Pan, Z., Yao, Y., and Li, C. (2015). Mineral Occurrence and its Impact on Fracture Generation in Selected Qinshui Basin Coals: An Experimental Perspective. *Int. J. Coal Geology.* 150-151, 35–50. doi:10.1016/j.coal.2015.08.006

Canfield, D. E. (1994). Factors Influencing Organic Carbon Preservation in marine Sediments. *Chem. Geology.* 114, 315–329. doi:10.1016/0009-2541(94)90061-2

Carroll, A. R., and Bohacs, K. M. (1999). Stratigraphic Classification of Ancient Lakes: Balancing Tectonic and Climatic Controls. *Geol* 27, 99–102. doi:10.1130/0091-7613(1999)027<0099:scoalb>2.3.co;2

Chen, C., Mu, C.-L., Zhou, K.-K., Liang, W., Ge, X.-Y., Wang, X.-P., et al. (2016). The Geochemical Characteristics and Factors Controlling the Organic Matter Accumulation of the Late Ordovician-Early Silurian Black Shale in the Upper Yangtze Basin, South China. *Mar. Pet. Geology.* 76, 159–175. doi:10.1016/j.marpetgeo.2016.04.022

Chen, F., Zhao, H., Lu, S., Ding, X., and Ju, Y. (2019a). The Effects of Composition, Laminar Structure and Burial Depth on Connected Pore Characteristics in a Shale Oil Reservoir, the Raoyang Sag of the Bohai Bay Basin, China. *Mar. Pet. Geology.* 101, 290–302. doi:10.1016/j.marpetgeo.2018.12.012

Chen, F., Zheng, Q., Lu, S., Ding, X., Ju, Y., and Zhao, H. (2019b). Classification of the Tight Oil Reservoir Storage Space in the Raoyang Sag of the Jizhong Depression in the Bohai Bay Basin, China. *Energy Sci. Eng.* 8, 74–88. doi:10.1002/ese3.510

Chermak, J. A., and Schreiber, M. E. (2014). Mineralogy and Trace Element Geochemistry of Gas Shales in the United States: Environmental Implications. *Int. J. Coal Geology.* 126, 32–44. doi:10.1016/j.coal.2013.12.005

Ding, X., Liu, G., Zha, M., Huang, Z., Gao, C., Lu, X., et al. (2015). Relationship between Total Organic Carbon Content and Sedimentation Rate in Ancient Lacustrine Sediments, a Case Study of Erlian basin, Northern China. *J. Geochemical Exploration* 149, 22–29. doi:10.1016/j.gexplo.2014.11.004

Dymond, J., Suess, E., and Lyle, M. (1992). Barium in Deep-Sea Sediment: A Geochemical Proxy for Paleoproductivity. *Paleoceanography* 7, 163–181. doi:10.1029/92pa00181

Fedo, C. M., Wayne Nesbitt, H., and Young, G. M. (1995). Unraveling the Effects of Potassium Metasomatism in Sedimentary Rocks and Paleosols, with Implications for Paleoweathering Conditions and Provenance. *Geol* 23, 921–924. doi:10.1130/0091-7613(1995)023<0921:uteopm>2.3.co;2

Feng, Q., Xu, S., Xing, X., Zhang, W., and Wang, S. (2020). Advances and Challenges in Shale Oil Development: A Critical Review. *Adv. Geo-energy Res.* 4, 406–418. doi:10.46690/ager.2020.04.06

Fu, J., Li, S., Xu, L., and Niu, X. (2018). Paleo-sedimentary Environmental Restoration and its Significance of Chang 7 Member of Triassic Yanchang Formation in Ordos Basin, NW China. *Pet. Exploration Dev.* 45, 998–1008. doi:10.1016/s1876-3804(18)30104-6

Hatch, J. R., and Leventhal, J. S. (1992). Relationship between Inferred Redox Potential of the Depositional Environment and Geochemistry of the Upper Pennsylvanian (Missourian) Stark Shale Member of the Dennis Limestone, Wabaunsee County, Kansas, U.S.A. *Chem. Geology.* 99, 65–82. doi:10.1016/0009-2541(92)90031-y

He, F., Gao, X., Zhao, X., Yang, D., Wang, Q., Fan, B., et al. (2017a). The Lower Part of the First Member of the Shahejie Formation (Es1x) as a Source Rock for Oil Found in Lixian Slope, Raoyang Sag, Bohai Bay Basin, Northern China. *ARAB J. GEOSCI.* 10, 101. doi:10.1007/s12517-017-2890-7

He, J., Ding, W., Jiang, Z., Jiu, K., Li, A., and Sun, Y. (2017b). Mineralogical and Chemical Distribution of the Es3L Oil Shale in the Jiyang Depression, Bohai Bay Basin (E China): Implications for Paleoenvironmental Reconstruction and Organic Matter Accumulation. *Mar. Pet. Geology.* 81, 196–219. doi:10.1016/j.marpetgeo.2017.01.007

He, T., Lu, S., Li, W., Tan, Z., and Zhang, X. (2018). Effect of Salinity on Source Rock Formation and its Control on the Oil Content in Shales in the Hetaoyuan Formation from the Biyang Depression, Nanxiang Basin, Central China. *Energy Fuels* 32, 6698–6707. doi:10.1021/acs.energyfuels.8b01075

Holditch, S. A. (2013). Unconventional Oil and Gas Resource Development - Let's Do it Right. *J. Unconventional Oil Gas Resour.* 1-2, 2–8. doi:10.1016/j.juogr.2013.05.001

Huerta-Diaz, M. A., and Morse, J. W. (1992). Pyritization of Trace Metals in Anoxic marine Sediments. *Geochimica et Cosmochimica Acta* 56, 2681–2702. doi:10.1016/0016-7037(92)90353-k

Jarvie, D. M. (2012). Shale Resource Systems for Oil and Gas: Part 2—Shale-Oil Resource Systems. *AAPG Mem.* 97, 89–119.

Jones, B., and Manning, D. A. C. (1994). Comparison of Geochemical Indices Used for the Interpretation of Palaeoredox Conditions in Ancient Mudstones. *Chem. Geology.* 111, 111–129. doi:10.1016/0009-2541(94)90085-x

Ju, Y., Sun, Y., Tan, J., Bu, H., Han, K., Li, X., et al. (2018). The Composition, Pore Structure Characterization and Deformation Mechanism of Coal-Bearing Shales from Tectonically Altered Coalfields in Eastern china. *Fuel* 234, 626–642. doi:10.1016/j.fuel.2018.06.116

Katz, B. J. (2003). Hydrocarbon Shows and Source Rocks in Scientific Ocean Drilling. *Int. J. Coal Geology.* 54, 139–154. doi:10.1016/s0166-5162(03)00028-4

Kelts, K., and Hsü, K. J. (1978). "Freshwater Carbonate Sedimentation," in *Lakes: Chemistry, Geology, Physics*. Editor A. Lerman (Berlin: Springer-Verlag), 295–323. doi:10.1007/978-1-4757-1152-3_9

Kidder, D. L., Erwin, D. H., Erwin, D., and Xa, H. (2001). Secular Distribution of Biogenic Silica through the Phanerozoic: Comparison of Silica-Replaced Fossils

and Bedded Cherts at the Series Level. *J. Geology.* 109, 509–522. doi:10.1086/320794

Kochenov, A. V., Korolev, K. G., Dubinchuk, V. T., and Medvedev, Y. L. (1977). Experimental Data on the Conditions of Precipitation of Uranium from Aqueous Solutions. *Geochem. Int.* 14, 82–87.

Larsen, C. P. S., and Macdonald, G. M. (1993). Lake Morphometry, Sediment Mixing and the Selection of Sites for fine Resolution Palaeoecological Studies. *Quat. Sci. Rev.* 12, 781–792. doi:10.1016/0277-3791(93)90017-g

Li, J., Lu, S., Cai, J., Zhang, P., Xue, H., and Zhao, X. (2018). Adsorbed and Free Oil in Lacustrine Nanoporous Shale: A Theoretical Model and a Case Study. *Energy Fuels* 32, 12247–12258. doi:10.1021/acs.energyfuels.8b02953

Li, J., Lu, S., Xie, L., Zhang, J., Xue, H., Zhang, P., et al. (2017a). Modeling of Hydrocarbon Adsorption on continental Oil Shale: A Case Study on N-Alkane. *Fuel* 206, 603–613. doi:10.1016/j.fuel.2017.06.017

Li, J., Lu, S., Xue, H., Xie, L., and Zhang, P. (2015b). Quantitative Evaluation on the Elastic Property of Oil-Bearing Mudstone/shale from a Chinese continental basin. *Energy Exploration & Exploitation* 33, 851–868. doi:10.1260/0144-5987.33.6.851

Li, J., Wang, W., Cao, Q., Shi, Y., Yan, X., and Tian, S. (2015a). Impact of Hydrocarbon Expulsion Efficiency of continental Shale upon Shale Oil Accumulations in Eastern China. *Mar. Pet. Geol.* 59, 467–479.

Li, J., Yang, Z., Wu, S., and Pan, S. (2021). Key Issues and Development Direction of Petroleum Geology Research of Source Rock Strata in China. *Adv. Geo-energy Res.* 5, 121–126. doi:10.46690/ager.2021.02.02

Li, T., Jiang, Z., Li, Z., Wang, P., Xu, C., Liu, G., et al. (2017b). Continental Shale Pore Structure Characteristics and Their Controlling Factors: A Case Study from the Lower Third Member of the Shahejie Formation, Zhanhua Sag, Eastern China. *J. Nat. Gas Sci. Eng.* 45, 670–692. doi:10.1016/j.jngse.2017.06.005

Li, Y., Wang, Z., Gan, Q., Niu, X., and Xu, W. (2019). Paleoenvironmental Conditions and Organic Matter Accumulation in Upper Paleozoic Organic-Rich Rocks in the East Margin of the Ordos basin, china. *Fuel* 252, 172–187. doi:10.1016/j.fuel.2019.04.095

Liang, C., Wu, J., Jiang, Z., Cao, Y., and Song, G. (2018). Sedimentary Environmental Controls on Petrology and Organic Matter Accumulation in the Upper Fourth Member of the Shahejie Formation (Paleogene, Dongying Depression, Bohai Bay Basin, China). *Int. J. Coal Geology.* 186, 1–13. doi:10.1016/j.coal.2017.11.016

Loucks, R. G., and Ruppel, S. C. (2007). Mississippian Barnett Shale: Lithofacies and Depositional Setting of a Deep-Water Shale-Gas Succession in the Fort Worth Basin, Texas. *Bulletin* 91, 579–601. doi:10.1306/11020606059

Lu, S., Huang, W., Chen, F., Li, J., Wang, M., Xue, H., et al. (2012). Classification and Evaluation Criteria of Shale Oil and Gas Resources: Discussion and Application. *Pet. Exploration Dev.* 39, 268–276. doi:10.1016/s1876-3804(12)60042-1

Lu, S., Xue, H., Wang, M., Xiao, D., Huang, W., Li, J., et al. (2016). Several Key Issues and Research Trends in Evaluation of Shale Oil. *ACTA PETROL. SIN* 37, 1309–1322.

Murphy, A. E., Sageman, B. B., Hollander, D. J., Lyons, T. W., and Brett, C. E. (2000). Black Shale Deposition and Faunal Overturn in the Devonian Appalachian Basin: Clastic Starvation, Seasonal Water-Column Mixing, and Efficient Biolimiting Nutrient Recycling. *Paleoceanography* 15, 280–291. doi:10.1029/1999pa000445

Nesbitt, H. W., and Young, G. M. (1982). Early Proterozoic Climates and Plate Motions Inferred from Major Element Chemistry of Lutites. *Nature* 299, 715–717. doi:10.1038/299715a0

Nesbitt, H. W., and Young, G. M. (1984). Prediction of Some Weathering Trends of Plutonic and Volcanic Rocks Based on Thermodynamic and Kinetic Considerations. *Geochimica et Cosmochimica Acta* 48, 1523–1534. doi:10.1016/0016-7037(84)90408-3

Pedersen, T. F., and Calvert, S. E. (1990). Anoxia vs. Productivity: what Controls the Formation of Organic-Carbon-Rich Sediments and Sedimentary Rocks? *AAPG Bull.* 74, 454–466. doi:10.1306/0C9B232B-1710-11D7-8645000102C1865D

Price, J. R., and Velbel, M. A. (2003). Chemical Weathering Indices Applied to Weathering Profiles Developed on Heterogeneous Felsic Metamorphic Parent Rocks. *Chem. Geology.* 202, 397–416. doi:10.1016/j.chemgeo.2002.11.001

Rimmer, S., Thompson, J., Goodnight, S., and Robl, T. (2004). Multiple Controls on the Preservation of Organic Matter in Devonian-Mississippian marine Black Shales: Geochemical and Petrographic Evidence. *Palaeogeogr. Palaeoclimatol. Palaeoecol.* 215, 125–154. doi:10.1016/s0031-0182(04)00466-3

Roy, D. K., and Roser, B. P. (2013). Climatic Control on the Composition of Carboniferous-Permian Gondwana Sediments, Khalaspir basin, Bangladesh. *Gondwana Res.* 23, 1163–1171. doi:10.1016/j.gr.2012.07.006

Sarnthein, M., Pflaumann, U., and Wang, P. (1994). Preliminary Report on Sonne-95 Cruise "Monitor Monsoon" to the south China Sea. *Rep. Geol.—Palaontol. Insitut Univ. Kiel* 68, 1–125.

Schieber, J. (1989). Facies and Origin of Shales from the Mid-proterozoic Newland Formation, Belt Basin, Montana, USA. *Sedimentology* 36, 203–219. doi:10.1111/j.1365-3091.1989.tb00603.x

Shekarifard, A., Daryabandeh, M., Rashidi, M., Hajian, M., and Röth, J. (2019). Petroleum Geochemical Properties of the Oil Shales from the Early Cretaceous Garau Formation, Qalikuh Locality, Zagros Mountains, Iran. *Int. J. Coal Geology.* 206, 1–18. doi:10.1016/j.coal.2019.03.005

Shen, J., Zhang, E., and Xia, W. (2001). Records from lake Sediments of the Qinghai lake to Mirror Climatic and Environmental Changes of the Past. *J. QUATERNARY SCI.* 21, 508–513.

Slatt, R. M., and Rodriguez, N. D. (2012). Comparative Sequence Stratigraphy and Organic Geochemistry of Gas Shales: Commonality or Coincidence? *J. Nat. Gas Sci. Eng.* 8, 68–84. doi:10.1016/j.jngse.2012.01.008

Taylor, S. R., and Mclennan, S. M. (1985). The Continental Crust: Its Composition and Evolution *J. Geol.* 94, 57–72.

Taylor, S. R. (1964). Abundance of Chemical Elements in the continental Crust: a New Table. *Geochimica et Cosmochimica Acta* 28, 1273–1285. doi:10.1016/0016-7037(64)90129-2

Tribovillard, N., Algeo, T. J., Lyons, T., and Riboulleau, A. (2006). Trace Metals as Paleoredox and Paleoproductivity Proxies: An Update. *Chem. Geology.* 232, 12–32. doi:10.1016/j.chemgeo.2006.02.012

Tribovillard, N. P., Caulet, J. P., Vergnaud-Grazzini, C., Moureau, N., and Tremblay, P. (1996). Geochemical Study of a Glacial–Interglacial Transition in the Upwelling Influenced Somalia Margin, N-W Indian Ocean: An Unexpected Lack of Organic Matter Accumulation. *Mar. Geol.* 133, 157–182

Wang, C., Wang, Q., Chen, G., He, L., Xu, Y., Chen, L., et al. (2017). Petrographic and Geochemical Characteristics of the Lacustrine Black Shales from the Upper Triassic Yanchang Formation of the Ordos Basin, China: Implications for the Organic Matter Accumulation. *Mar. Pet. Geology.* 86, 52–65. doi:10.1016/j.marpetgeo.2017.05.016

Wang, M., Wilkins, R. W. T., Song, G., Zhang, L., Xu, X., Li, Z., et al. (2015). Geochemical and Geological Characteristics of the Es3L Lacustrine Shale in the Bonan Sag, Bohai Bay Basin, China. *Int. J. Coal Geology.* 138, 16–29. doi:10.1016/j.coal.2014.12.007

Wang, Y., Guo, W., and Zhang, G. (1979). Application of Some Geolochemical Indicators in Determining of Sedimentary Environment of the Funing Group (Paleogene), Jinhu Depression, Jiangsu Province. *J. Tongji Univ:nat Sci. Ed.* 2, 51–60.

Wang, Y., and Wu, P. (1983). Geochemical Markers of Coastal Sediments in Jiangsu and Zhejiang Provinces. 11. *J. Tongji Univ:nat Sci. Ed.* 4, 79–87.

Wei, Y., Li, J., Du, Y., Lu, S., Li, W., Yang, J., et al. (2021b). Classification Evaluation of Gas Shales Based on High-Pressure Mercury Injection: A Case Study on Wufeng and Longmaxi Formations in Southeast Sichuan, China. *Energy Fuels* 35, 9382–9395. doi:10.1021/acs.energyfuels.1c00973

Wei, Y., Li, J., Lu, S., Song, Z., Zhao, R., Zhang, Y., et al. (2021a). Comprehensive Evaluation Method of Sweet Spot Zone in Lacustrine Shale Oil Reservoir and its Application: A Case Study of Shale Oil in Lower 1st Member of the Shahejie Formation in the Raoyang Sag. *J. CHINA U MIN TECHNO* 4, 1–12.

Wignall, P. B., and Twitchett, R. J. (1996). Oceanic Anoxia and the End Permian Mass Extinction. *Science* 272, 1155–1158. doi:10.1126/science.272.5265.1155

Wilson, M. J., Shaldybin, M. V., and Wilson, L. (2016). Clay Mineralogy and Unconventional Hydrocarbon Shale Reservoirs in the USA. I. Occurrence and Interpretation of Mixed-Layer R3 Ordered Illite/smectite. *Earth-Science Rev.* 158, 31–50. doi:10.1016/j.earscirev.2016.04.004

Xiong, G., Jiang, X., Cai, X., and Wu, H. (2010). The Characteristics of Trace Element and REE Geochemistry of the Cretaceous Mudrocks and Shales from Southern Tibet and its Analysis of Redox Condition. *Adv. Earth Sci.* 25, 730–745.

Xu, S., Zhai, S., Zhang, A., Zhang, X., and Zhang, H. (2007). Distribution and Environment Significance of Redox Sensitive Trace Elements of the Changjiang Estuary Hypoxia Zone and its Contiguous Sea Area. *Acta Sedimentologica Sinica* 2007, 759–766.

Ye, L., Zhu, X., Zhang, R., Xie, S., Gao, Y., Tang, H., et al. (2020). Sedimentary Environment of Shallow-Water delta and beach-bar of the Member 1 of Shahejie Formation in Lixian Slope of Raoyang Sag, Jizhong Depression. *J. Palaeogeog-chinese* 22, 587–600.

Yin, J., Wang, Q., Hao, F., Guo, L., and Zou, H. (2018). Palaeoenvironmental Reconstruction of Lacustrine Source Rocks in the Lower 1st Member of the Shahejie Formation in the Raoyang Sag and the Baxian Sag, Bohai Bay Basin, eastern China. *Palaeogeogr. Palaeoclimatol. Palaeoecol.* 495, 87–104.

Yin, J., Hao, F., Wang, Z., Chen, X., and Zou, H. (2020). Lacustrine Conditions Control on the Distribution of Organic-Rich Source Rocks: An Instance Analysis of the Lower 1st Member of the Shahejie Formation in the Raoyang Sag, Bohai Bay Basin. *J. Nat. Gas Sci. Eng.* 78, 103320. doi:10.1016/j.jngse.2020.103320

Zhang, S., Chen, S., Pu, X., Wang, Y., and Tan, M. (2016). Lithofacies Types and Reservoir Characteristics of fine-grained Sedimentary Rocks in Paleogene, Southern Bohai Fault-Depressed Lacustrine basin. *J. CHINA U MIN TECHNO* 45, 568–581.

Zhao, J., Jin, Z., Jin, Z., Geng, Y., Wen, X., and Yan, C. (2016). Applying Sedimentary Geochemical Proxies for Paleoenvironment Interpretation of Organic-Rich Shale Deposition in the Sichuan Basin, China. *Int. J. Coal Geology.* 163, 52–71. doi:10.1016/j.coal.2016.06.015

Zhou, L., Han, G., Ma, J., Chen, C., Yang, F., Zhang, L., et al. (2020). Geological Characteristics and Exploration Breakthrough of Shale Oil in Member 3 of Shahejie Formation of Qibei Subsag, Qikou Sag. *ACTA PETROL. SIN* 41, 903–917.

Zou, C. (2017). *Unconventional Petroleum Geology*. second ed. Elsevier, 275–321. doi:10.1016/b978-0-12-812234-1.00010-8Shale Oil and Gas

Zou, C., Yang, Z., Zhu, R., Wu, S., Fu, J., Lei, D., et al. (2019). Geologic Significance and Optimization Technique of Sweet Spots in Unconventional Shale Systems. *J. Asian Earth Sci.* 178, 3–19. doi:10.1016/j.jseaes.2018.07.005

Conflict of Interest: XyL, RZ, XdL, YQ, TJ, YG, TZ, and MZ are employed by PetroChina.

The remaining authors declare that the research was conducted in the absence of any commercial or financial relationships that could be construed as a potential conflict of interest.

Publisher's Note: All claims expressed in this article are solely those of the authors and do not necessarily represent those of their affiliated organizations, or those of the publisher, the editors and the reviewers. Any product that may be evaluated in this article, or claim that may be made by its manufacturer, is not guaranteed or endorsed by the publisher.